

AR77-3

Aeronautical Report 77-3

NASA-CR-197497  
19950002355

Experimental Studies of Flow Separation of the  
NACA 2412 Airfoil at Low Speeds

N95-70475

Unclas

Z9/02 0033895

P-69

by

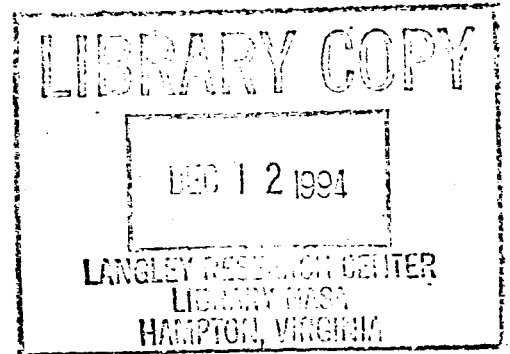
(NASA-CR-197497) EXPERIMENTAL  
STUDIES OF FLOW SEPARATION OF THE  
NACA 2412 AIRFOIL AT LOW SPEEDS  
Final Technical Report (Wichita  
State Univ.) 69 p

H. C. Seetharam,  
E. J. Rodgers,  
and  
W. H. Wentz, Jr.

Aeronautical Engineering Department  
Wichita State University  
Wichita, Kansas

October 1977

Final Technical Report of Research Conducted  
under Expansion of NGR 17-003-021 Phase II, for the  
NASA Langley Research Center



Experimental Studies of Flow Separation of the  
NACA 2412 Airfoil at Low Speeds

by

H. C. Seetharam,

E. J. Rodgers,

and

W. H. Wentz, Jr.

Aeronautical Engineering Department

Wichita State University

Wichita, Kansas

October 1977

Final Technical Report of Research Conducted  
under Expansion of NGR 17-003-021 Phase II, for the  
NASA Langley Research Center

N95-70475#

## SUMMARY

Wind tunnel tests have been conducted on an NACA 2412 airfoil section at Reynolds number of  $2.2 \times 10^6$  and Mach number of 0.13. Detailed measurements of flow fields associated with turbulent boundary layers have been obtained at angles of attack of  $12.4^\circ$ ,  $14.4^\circ$ , and  $16.4^\circ$ . Pre- and post-separated velocity and pressure survey results over the airfoil and in the associated wake are presented. Extensive force, pressure, tuft survey, hot-film survey, local skin friction and boundary layer data are also included.

Pressure distributions and separation point locations show good agreement with theory for the two lower angles of attack. Boundary layer displacement thickness, momentum thickness and shape factor agree well with theory up to the point of separation. There is considerable disparity between extent of flow reversal in the wake as measured by pressure and hot-film probes. The difference is attributed to the intermittent nature of the flow reversal.

## INTRODUCTION

NASA Langley has sponsored experimental research work on airfoil separated flow fields at Wichita State University since 1974. To date detailed flow field data for the GA(W)-1 with flap nested (Ref. 1) and Fowler flap deployed (Refs. 2, 3 and 4) have been obtained. Prior to the present report, experimental separated flow research has been restricted to investigations of the 17% thick GA(W)-1 airfoil. The data of Reference 1 has provided new directions in formulating mathematical models for separated flows (Ref. 5). In order to broaden the base of experimental data it was considered important to obtain additional experimental data for an older NACA airfoil section, one having a different thickness and camber distributions than the GA(W)-1. With this objective in mind a NACA 2412 airfoil model was selected for the separated flow research of this report.

It is anticipated that the results of this research will provide an additional data base for formulating a universal mathematical model of separated flow fields associated with airfoils.

## SYMBOLS

To the maximum extent possible, physical measurements are presented in non-dimensional form. Dimensional quantities are given in both International (SI) Units and U.S. Customary Units. All measurements were made in U.S. Customary Units. Conversion factors between SI Units and U.S. Customary Units are given in Reference 6. The following symbols are used in the present report:

$c$  Wing chord

$c_d$  Airfoil section drag coefficient,  $\frac{\text{section drag}}{q_\infty c}$

$c_f'$  Local skin friction coefficient,  $\frac{\tau}{q_\infty}$

$c_l$	Airfoil section lift coefficient, $\frac{\text{section lift}}{q_\infty c}$
$c_m$	Airfoil section pitching moment coefficient with respect to .25c location, $\frac{\text{section moment}}{q_\infty c^2}$
$c_{ps}$	Static pressure coefficient, $\frac{p_s - p_\infty}{q_\infty}$
$c_{pt}$	Total pressure coefficient, $\frac{p_t - p_\infty}{q_\infty}$
H	Shape factor ( $\delta^*/\delta^{**}$ )
h	Razor blade thickness/2
$p_s$	Local static pressure
$p_t$	Local total pressure
$p_\infty$	Free stream static pressure
$q_\infty$	Free stream dynamic pressure
RN	Reynolds number based on wing chord and free-stream conditions
T	Turbulence intensity
U	Velocity at the edge of the boundary layer, non-dimensionalized with respect to free-stream velocity
u	Local velocity non-dimensionalized with respect to free stream velocity, $\sqrt{\frac{p_t - p_s}{q_\infty}}$
$u_x$	Non-dimensionalized component of local velocity in the free stream direction
x	Streamwise coordinate
z	Vertical coordinate
$\alpha$	Angle of attack, degrees
$\Delta p$	Pressure difference between the pressure reading with blade in position and the true undisturbed static pressure
$\delta$	Boundary layer thickness

- $\delta^*$  Boundary layer displacement thickness,  $\int_0^{\delta} (1 - \frac{u}{U}) dz$
- $\delta^{**}$  Boundary layer momentum thickness,  $\int_0^{\delta} \frac{u}{U} (1 - \frac{u}{U}) dz$
- $\tau$  Shear stress

## APPARATUS AND PROCEDURE

### Tests

The experimental investigations were carried out in the WSU 213 cm x 305 cm (7' x 10') low speed wind tunnel fitted with a 213 cm x 91.4 cm (7' x 3') two-dimensional insert employing a NACA 2412 airfoil section having a 61 cm (24") chord and a 91.4 cm (36") span (Fig. 1). The airfoil was fitted with a 1.07 mm (0.042") I.D. stainless steel surface static pressure taps distributed along the mid-span section. The flow field surveys were conducted at angles of attack of 12.4°, 14.4° and 16.4° which represent pre-stall, stall, and post-stall conditions respectively. Reynolds number of the test was  $2.2 \times 10^6$  based on the airfoil chord and Mach number was 0.13. Transition was ensured by employing 2.5 mm (0.1") wide strips of #80 carborundum grit at 0.05c on both upper and lower surfaces. In this test series details of flow field were investigated only on the upper surface of the model, and in the wake. At each angle of attack about fourteen chordwise survey stations were selected covering the airfoil upper surface and the wake.

Basic force measurements, surface pressure and local skin friction distributions, flow visualization and hot-film surveys were also obtained to supplement the flow field data.

### Instrumentation

Velocities at heights more than 2.5 mm (.10") above the local surface of the airfoil were obtained by employing a

five-tube pressure sensing pitch-yaw probe of 3.175 mm (0.125") diameter (Fig. 2). Velocities very close to the wall and in regions of flow reversal were obtained by a four-tube probe having a pair of pitot and static tubes positioned 180° apart along the tube axis (Fig. 3). The axis of the static tube was located at a height of 0.25 mm (0.01") above the pitot-tube axis. Four- and five-tube probes were mounted in tandem, straddling the model centerline, spaced 7.62 cm (3") on either side of the centerline.

Hot-film surveys were conducted to scan the regions of moderate and heavy turbulence employing a Thermo Systems, Inc., 0.05 mm (.002") diameter probe with linearizer (Fig. 4).

Local skin friction was measured by the technique outlined by East (Ref. 7) employing commercially available razor blades of 0.1 mm (0.0041") thickness. Each blade was trimmed to a 6.4 x 6.4 mm (0.25" x 0.25") square and positioned at the surface static port location where the local skin friction was to be evaluated. Details of the razor blade dimensions are given in Figure 5.

Unbonded strain gage pressure transducers with a range of  $\pm 17.2$  kilo-newtons/m<sup>2</sup> ( $\pm 2.5$  psi) were used for all pressure measurements. All pressure measurements were recorded on punch cards.

## Methods

Lift and moment data were obtained from the tunnel main balance system. The drag was calculated from wake surveys measured at the 0.5c station downstream from the trailing edge. Flow velocity data were acquired by initially tilting the four- and five-tube probes to align with the local slope of the surface. Near-wall velocity data were obtained from the four-tube probe readings. For distances more than 2.5 mm above the surface, the five-tube pressure readings were used to obtain total and static pressure, as well as local upwash angle through appropriate calibration curves.

Flow reversal was indicated by observing the higher reading from the forward- and aft-facing total tubes on the four-tube probe. The data reduction program selected flow direction based upon these readings, and utilized the appropriate static pressure tube reading to calculate velocity. Thus the four-tube probe readings were utilized for stations very near the wall, where five-tube data could not be obtained, and for regions of reversed flow. Attempts to obtain readings by rotating the five-tube probe  $180^\circ$  in yaw for regions of flow reversal were unsatisfactory. The data usually indicated flow direction opposite to probe direction for both forward and reversed positions. The four-tube probe gave reasonably consistent results. The discrepancies between the two instruments are attributed to the unsteady nature of the reversed flow, and the high damping characteristics of the five-tube probe. Measurements in the wake were made with the probes aligned in the free-stream direction (zero tilt).

Tuft surveys and oil flow methods were employed for observation of the surface flow patterns and determination of the separation point.

Hot-film surveys were made with the traversing mechanism employed for the four- and five-tube surveys. Photos of the velocity fluctuations displayed on the oscilloscope were also recorded.

Local skin friction was measured by positioning the razor blade as shown in Figure 5. This method involves relating the skin friction ( $\tau$ ) to the difference between the pressure recorded by the static hole with the blade in position, and the true undisturbed local surface static pressure (blade removed). Details of geometrical limitations and calibration are given in Reference 7. Important dimensions are tabulated in Figure 5, for the present experimental set-up.

## Data Reduction

Force data, with usual wind tunnel boundary corrections, surface pressures, local velocities and flow inclinations were calculated from the measured wind tunnel raw data by computer routines developed for the IBM 1130 and 360 computers at WSU. The local velocity is expressed in a non-dimensional form as the ratio of local to free stream velocity. Experimental velocity profiles were plotted by a computer routine written for the IBM 1130 computer.

Calibration of the five-tube probe is discussed in detail in Reference 8. All the pressure instrumentation employed in the present tests is heavily damped and therefore records time-averaged values.

Typical oscilloscope traces from the hot-film probe were photographically recorded. Digital volt meter readings of the hot-film probe data were recorded manually. The hot-film was calibrated from time to time during the course of the tests to compensate for wind tunnel temperature variations. Maximum calibration shifts amounted to 6% of free stream velocity.

The pressure difference  $\Delta p$ , between the surface pressure recorded by the static port with the blade in position and the undisturbed static pressure, is related to the skin friction  $\tau$  by a calibration equation given in Reference 7. The data reduction program utilizes this equation to calculate the local skin friction coefficient.

## RESULTS

### Presentation of Results

The results of the present investigation are presented in figures as tabulated below:

Table 1 - List of Figures

<u>Type data</u>	<u>Instrument</u>	<u><math>\alpha</math></u>	<u>Figures</u>
Airfoil geometry	---	---	1
Instrument details	---	---	2 to 5
Lift, drag and pitching moment	Force balance and wake probe	$-4^\circ$ to $+18^\circ$	6
Surface pressures	Surface tubes	$-4^\circ$ to $+16^\circ$	7
Surface flow	Tufts	$0^\circ$ to $20^\circ$	8
Velocity profiles	Five-tube and four-tube probes	$12.4^\circ$ , $14.4^\circ$ , $16.4^\circ$	9
Near-wall velocity profiles	Five-tube and four-tube probes	$12.4^\circ$ , $14.4^\circ$ , $16.4^\circ$	10
Static pressure profiles	Five-tube probe and surface pressure tubes	$12.4^\circ$ , $14.4^\circ$ , $16.4^\circ$	11
Static pressure field contours	Five-tube probe	$12.4^\circ$ , $14.4^\circ$ , $16.4^\circ$	12
Boundary layer displacement thickness	Five-tube probe	$12.4^\circ$ , $14.4^\circ$ , $16.4^\circ$	13
Boundary layer momentum thickness	Five-tube probe	$12.4^\circ$ , $14.4^\circ$ , $16.4^\circ$	14
Boundary layer shape factor	Five-tube probe	$12.4^\circ$ , $14.4^\circ$ , $16.4^\circ$	15
Displacement thickness	Five-tube probe	$12.4^\circ$ , $14.4^\circ$ , $16.4^\circ$	16
Separation streamline	Five-tube probe	$16.4^\circ$	17
Velocity and pressures in wake	Five-tube probe	$12.4^\circ$ , $14.4^\circ$ , $16.4^\circ$	18

Table 1 - (continued)

<u>Type data</u>	<u>Instrument</u>	<u><math>\alpha</math></u>	<u>Figures</u>
Total pressure contours in wake	Five-tube probe	12.4°, 14.4°, 16.4°	19
Hot-film field surveys	Hot-film anemometer	12.4°, 14.4°, 16.4°	20
Skin friction	Razor blade	0.2°, 12.4°, 14.4°, 16.4°	21

### Discussion

Forces: (Figure 6). These tests were conducted primarily to supplement the flow field data and to provide additional data at low Reynolds number with NASA standard roughness.

Results of the lift, drag and pitching moment measurements are shown along with the experimental data at Reynolds numbers of  $3.1 \times 10^6$  and  $5.7 \times 10^6$  from Reference 9. It can be seen from Figure 6a that present experimental results of the lift coefficient for the clean model do not agree with the clean model data of Reference 9. A difference in the maximum lift coefficient of 0.15 can be seen between the NACA  $3.1 \times 10^6$  RN and the WSU  $2.2 \times 10^6$  RN clean data. This difference appears to be rather large for a difference in Reynolds number of  $1 \times 10^6$ . The reason for this difference is unknown. The differences between NACA data and WSU data with grit are expected since the NACA grit was larger and was applied over a much larger region, causing severe losses in  $C_{l_{max}}$  and corresponding increases in drag at high lift coefficients. The experimental drag and pitching moment data (Figures 6a and 6c) agree reasonably well with the results of Reference 9.

Pressure Distributions: (Figure 7). Surface pressure distributions for an angle of attack range from  $-3.9^\circ$  to  $+12.4^\circ$  are shown in figure 7a. Figure 7b, 7c and 7d show pressure distributions at the  $12.4^\circ$ ,  $14.4^\circ$  and  $16.4^\circ$  conditions

selected for detailed flow studies in the present research. Theoretical pressure distributions from the method of Reference 10 are also given. Separation locations from flow visualization studies at these angles of attack are marked on the figures. It is seen that these locations appear quite consistent with the beginning of a region of constant pressure for each angle. Constancy of pressure is characteristic of separated flow regions.

Flow visualization studies: (Figure 8). Flow visualization studies were carried out by attaching tufts to the upper surface of the model. In order to study the influence of the side wall boundary layers on separation patterns, tufts were also applied to the side walls. No evidence of premature side wall separation was observed. Figure 8a shows the tuft photos for a nominal angle of attack range of  $0^\circ$  to  $12^\circ$ . The flow is very steady up to  $8^\circ$ . At  $12^\circ$  the last row of tufts is disturbed with a few tufts exhibiting reversal near the mid-span section. At  $14^\circ$  angle of attack (stall) separation progresses upstream with the last two rows of tufts (aft of 0.80 chord) showing reversal. Tufts at the 0.70 chord station are disturbed, with some tufts indicating possible intermittent reversal at near mid-span. The flow is reasonably two-dimensional (Figure 8b). At post-stall angles of attack ( $\alpha = 16^\circ, 18^\circ$  and  $20^\circ$ ) the regions of separation grow larger and larger and the flow pattern becomes asymmetric. Thus the extreme post-stall flow pattern appears to have a three-dimensional character. It is interesting to note that the tufts on the side walls are undisturbed.

Limited oil-flow studies were conducted at the pre-stall, stall and post-stall angles of attack, to obtain more detailed definition of separation locations than the tuft studies provide. Since the oil flow is heavily damped, the surface streak patterns tend to represent a mean separation location which is much more difficult to define from tuft

patterns. Results of the analysis of combined oil flow and tuft studies are given in Table 2, along with theoretical values calculated by the methods of Reference 10.

Table 2 - Separation

Angle of Attack	Experimental Separation Location from Oil and Tuft Studies	Theoretical Separation Location
12.4°	.925c	.92c
14.4°	.80c	.82c
16.4°	.40c	.65c

These observations are consistent with surface pressure distributions. These results are in contrast to separation patterns for the GA(W)-1 airfoil as reported in Reference 1. In the present case, the separation location moved forward 0.40c for a 2° change in angle of attack from 14.4° to 16.4°. In the case of the 17% thick GA(W)-1 section, an 8° change in angle of attack moved the separation location only 0.35c.

Velocity plots: (Figures 9 and 10). Computer plots of the measured velocity profiles at the mid-span section are shown in Figures 9a to 9c. The five-tube probe did not indicate reversed flow either on the airfoil surface or in the wake. In regions where reversed flow exists either the calibration limits of the probe were exceeded or the indicated local dynamic pressure was negative for probe yaw directions of both 0° and 180°.

Velocity profiles obtained from the four-tube probe are shown in Figures 10a to 10b, together with velocities obtained from the five-tube probe for certain z stations. It can be seen that four-tube and five-tube measurements in general agree

within  $\pm 5\%$  of the free stream velocity. The error appears to be the largest at the 0.10c station (Figure 10b). Discrepancies between the probe types do not follow any consistent pattern. It is believed that the transition strip contributes to unsteadiness and boundary layer profile distortions at the 0.10c and 0.20c stations.

The flow over the aft portion of an airfoil at stall and post-stall angles of attack is unsteady with intermittent reversing. The Appendix to this report compares velocity profile measurements as obtained by the two pressure probes used in the present tests and a high-response split-film anemometer used in subsequent separated flow research. These studies show that the turbulent fluctuations near reversal are large, but that the pressure probes indicate approximately the average velocity, and approximately the proper average reversal location.

Static Pressure Profiles: (Figure 11). Static pressure profiles at various chordwise stations on the airfoil shown in Figures 11a to 11c were obtained using the five-tube probe. The surface static pressures as extrapolated from this data show some disagreement with those measured by the surface static pressure ports with no probe present. Special runs to determine the magnitude of the probe interference were made when these effects were observed. These are discussed in appendix B. The runs showed that the probe creates an interference effect which results in slight changes in the separation point and associated changes in pressure levels at the post-stall angle. In some uses the surface static pressure coefficients changes as much as 0.25.

Static pressure contours: (Figure 12). Static pressure contours derived from the pressure distributions obtained at ten chordwise stations and four stations in the wake are shown. The characteristic high pressure plateau reported in Reference 1 can be seen in Figures 12a and 12b ( $\alpha = 12.4^\circ$  and  $14.4^\circ$ ). At the post-stall angle of attack of  $16.4^\circ$  (Figure 12c) however there is no indication of a high pressure region. A vertical

pressure gradient from lower surface region to upper surface is also observed in the wake.

Boundary layer characteristics: (Figures 13 through 17). The displacement and momentum thicknesses show substantial increases between pre-stall and post-stall conditions. The rapid growth of the shape factor prior to separation, typical of turbulent separated boundary layers, is clearly seen. A comparison between measured shape factors at separation and typical values of H (from Ref. 11) is shown in Table 3.

Table 3 - Shape Factors at Separation

Angle of Attack	Separation Point from Tuft and Oil Flow Observations	Measured Shape Factor H	Normally Expected Value of H
12.4°	.925c	2.12	1.8 to 2.2
14.4°	.80c	1.97	1.8 to 2.2
16.4°	.40c	1.53	1.8 to 2.2

It is seen that the values of 12.4° and 14.4° are within the normal range of values, while the shape factor at the 16.4° condition is below the normal value. This is believed to be caused by the characteristic post-stall turbulent fluctuations. Also it should be noted that the flow at this condition is somewhat three-dimensional.

The boundary layer displacement thickness superimposed on the airfoil is shown in Figure 16. It can be seen that the slope of the augmented surface follows the slope of the airfoil surface very closely up to the point of separation and diverges away depending on the depth of the separated layer. This trend is also exhibited by the separation streamline which is shown in Figure 17 for the angle of attack of 16.4°.

Velocity and pressure distributions in the wake: (Figures 18 and 19). Profiles of velocity, static and total pressure are shown for a vertical traverse range of  $\pm 0.2c$  at each chord-wise station. The progressive growth of the wake width in the longitudinal direction is seen as expected. Static pressure profiles exhibit a slight vertical pressure gradient in the direction of the lower surface. Progressive reduction of static pressure gradients in the wake can also be seen.

Total pressure profiles are very regular even at post-stall angles of attack. Contour plots of total pressure (Figures 19a to 19c) are similar at pre-stall, stall and post-stall conditions. Total pressure gradients become smaller at the post-stall angle of attack compared to the pre-stall angle of attack.

Reattachment point in the wake: An examination of the wake velocity profiles (Figures 18a to 18c) indicates the termination of regions of reversal within a relatively short distance downstream from the airfoil trailing edge. This point, which is characterized by a single zero velocity point in the velocity profile, is referred to as the "reattachment point." The points obtained by inspection of the velocity profiles are tabulated in the following table.

Table 4 - Reattachment Point Location

Angle of Attack	Reattachment Point
12.4°	$1.00 < x/c < 1.05$
14.4°	$1.00 < x/c < 1.05$
16.4°	$x/c \approx 1.2$

These results are consistent with the observations of Reference 1, which also showed that reattachment points for the GA(W)-1 airfoil were relatively close to the trailing edge.

Hot-film survey: (Figure 20). Maps of the regions with varying degrees of turbulence are shown. Typical oscilloscope traces of regions of reversal, heavy turbulence, moderate turbulence and smooth flow are also shown. Interpretation of the hot-film data for regions of reversal was done in the following manner. The flow was considered to be reversing whenever the trace indicated zero on the scope. At the outer edge of reversal zones, the flow may be intermittently reversing (less than 50% of the time), in view of the heavy turbulent mixing. Pressure instrumentation cannot follow the higher flow frequencies because of heavy damping. It is interesting to note that regions of reversal measured in this way extend further downstream than the results obtained from the heavily damped pressure probes. Regions of heavy turbulence extend far beyond  $0.50c$  downstream from the trailing edge for the case of post-stall angle of attack (Figure 20c), whereas for the cases of pre-stall and stall conditions, the regions of heavy turbulence terminate within  $0.30c$  downstream (Figures 20a and 20b).

Skin friction distributions: (Figure 21). Local skin friction measurements are compared with theoretical results calculated by the theoretical methods of Reference 7. At low angle of attack ( $\alpha = 0.2^\circ$ , Figure 21a) the upper surface experimental data show a somewhat higher level of skin friction than theory, while the lower surface data show excellent agreement with theory. At  $\alpha = 12.4^\circ$  (Figure 21b), the upper surface data show excellent agreement with theory, while the lower surface experimental data are somewhat higher than theory. At  $\alpha = 14.4^\circ$  and  $16.4^\circ$  (Figures 21c and 21d) the agreement between the theory and experiment is good for stations ahead of separation.

## CONCLUSIONS

1. Experimental velocity profiles, flow inclinations, static and total pressure distributions have been obtained for

the NACA 2412 airfoil, at pre-stall, stall, and post-stall angle of attack conditions.

2. Extensive mapping of the regions with varying degrees of turbulence was done employing a hot-film survey probe.

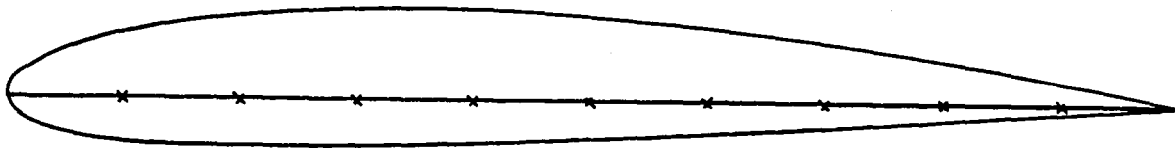
3. Surface pressure distributions, separation locations, displacement thickness, momentum thickness, shape factor and skin friction show reasonable agreement with theory up to the separation point. Post-separated values are not predicted by present theory.

4. Velocity measurements from the pressure-type probes indicate that the regions of reversed flow terminate at a re-attachment point which is located a relatively short distance (about  $0.05c$  to  $0.2c$ ) downstream from the airfoil trailing edge for the test range of angles of attack. The hot-film measurements reveal that intermittent reversal extends somewhat further downstream than pressure type probe data indicate, but even these regions are less than  $0.5c$  in length.

#### REFERENCES

1. Seetharam, H.C. and Wentz, W.H., Jr.: Experimental Studies of Flow Separation and Stalling on a Two-Dimensional Airfoil at Low Speeds. NASA CR-2560, July 1975.
2. Wentz, W.H., Jr., and Seetharam, H.C.: Development of a Fowler Flap System for a High Performance General Aviation Airfoil. NASA CR-2443, December 1974.
3. Seetharam, H.C. and Wentz, W.H., Jr.: A Low Speed Two-Dimensional Study of Flow Separation on the GA(W)-1 Airfoil with 30-Percent Chord Fowler Flap. NASA CR-2844, May 1977.
4. Wentz, W.H., Jr., Seetharam, H.C., and Fisco, K.A.: Force and Pressure Tests of the GA(W)-1 Airfoil with a 20% Aileron and Pressure Tests with a 30% Fowler Flap. NASA CR-2833, June 1977.
5. Naik, S.N. and Zumwalt, G.W.: An Analytical Model for the Study of Highly Separated Flow on Low Speed Airfoils, Wichita State University, Aeronautical Engineering Dept., AR 77-2, 1977 (in preparation as NASA CR report).
6. Mechtley, E.A.: The International System of Units--Physical Constants and Conversion Factors (Revised). NASA SP-7012, 1969.

7. East, L.F.: Measurement of Skin Friction at Low Subsonic Speeds by the Razor-Blade Technique. British R&M 3525.
8. Seetharam, H.C., Wentz, W.H., Jr., and Walker, J.K.: Measurement of Post-Separated Flowfields on Airfoils. Tech. Note, AIAA Jour. of Aircraft, Vol. 14, No. 1, Jan. 1977.
9. Abbott, I.H. and Von Doenhoff, A.E.: Theory of Wing Sections. Dover Publications, 1959.
10. NASA Langley Research Staff: Viscous Flow Single-Element Airfoil Analysis Computing Routine (Program Airfoil), 1976.
11. Schlichting, H.: Boundary Layer Theory, McGraw-Hill Co., Fourth Edition, 1962.



UPPER SURFACE		LOWER SURFACE	
x/c	z/c	x/c	z/c
0.0000	0.0000	0.0000	0.0000
-.0001	.0028	.0005	-.0028
.0005	.0056	.0015	-.0054
.0012	.0080	.0028	-.0076
.0020	.0098	.0040	-.0092
.0038	.0127	.0062	-.0117
.0060	.0155	.0090	-.0140
.0083	.0180	.0117	-.0160
.0130	.0220	.0170	-.0191
.0178	.0255	.0223	-.0215
.0274	.0312	.0326	-.0254
.0371	.0360	.0429	-.0283
.0469	.0401	.0531	-.0307
.0568	.0438	.0633	-.0327
.0666	.0471	.0734	-.0343
.0766	.0501	.0834	-.0358
.0865	.0529	.0935	-.0369
.0965	.0555	.1035	-.0380
.1165	.0600	.1235	-.0395
.1366	.0638	.1434	-.0407
.1568	.0671	.1633	-.0415
.1769	.0699	.1831	-.0420
.1971	.0723	.2029	-.0423
.2478	.0765	.2522	-.0422
.2985	.0788	.3015	-.0413
.3493	.0792	.3508	-.0398
.4000	.0780	.4000	-.0380
.4503	.0757	.4497	-.0360
.5006	.0724	.4994	-.0335
.5508	.0683	.5492	-.0308
.6010	.0634	.5990	-.0278
.6512	.0578	.6488	-.0248
.7012	.0516	.6988	-.0216
.7512	.0448	.7488	-.0184
.8012	.0373	.7988	-.0151
.8510	.0293	.8490	-.0118
.9008	.0206	.8992	-.0083
.9505	.0113	.9495	-.0049
1.0001	.0013	.9999	.0013

Figure 1 - Coordinates of 2412 Airfoil.

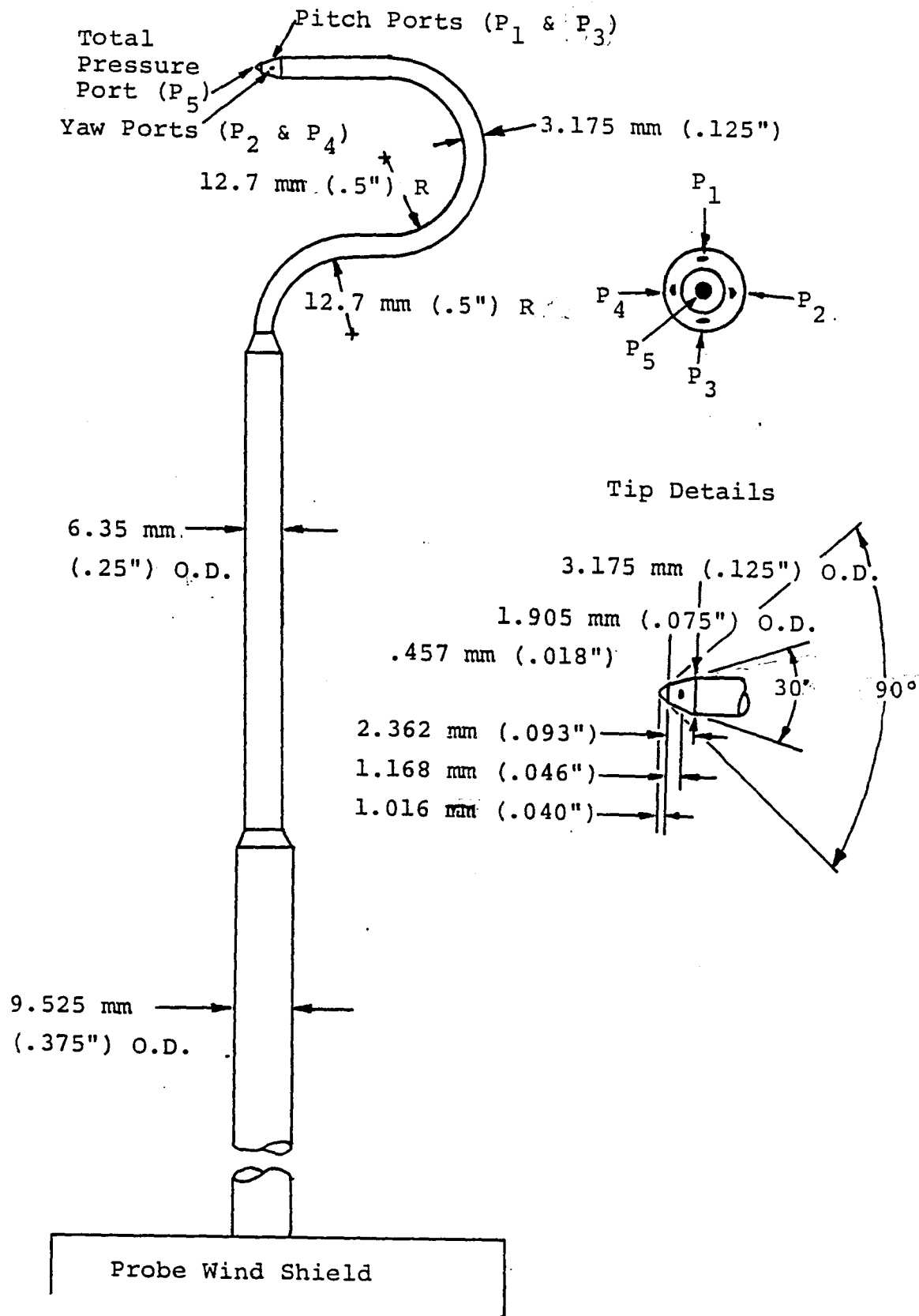
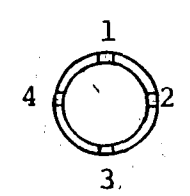
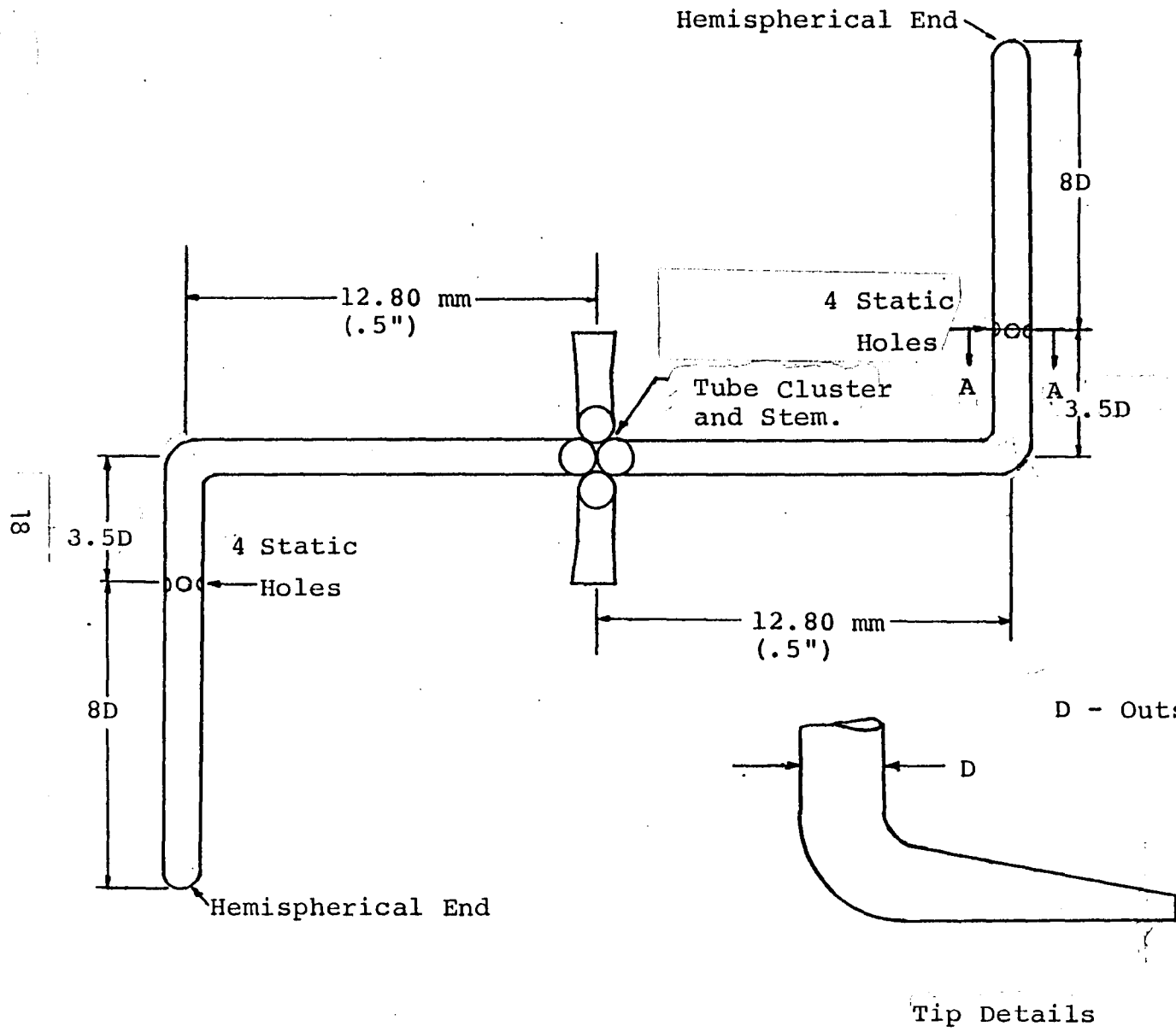


Figure 2 - Five Tube Probe.



Section AA  
 Static Pressure  
 Probe Details

D - Outside Diameter = 1.09 mm (.043")

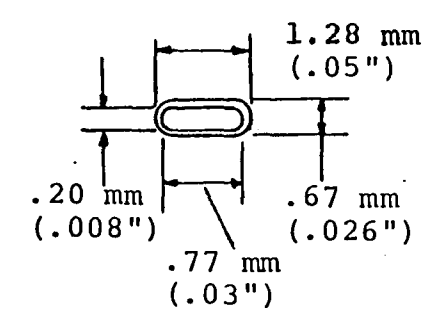
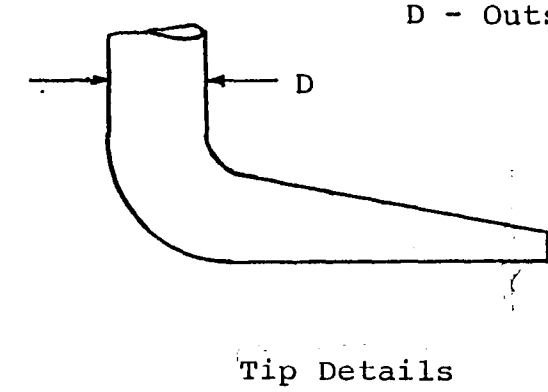
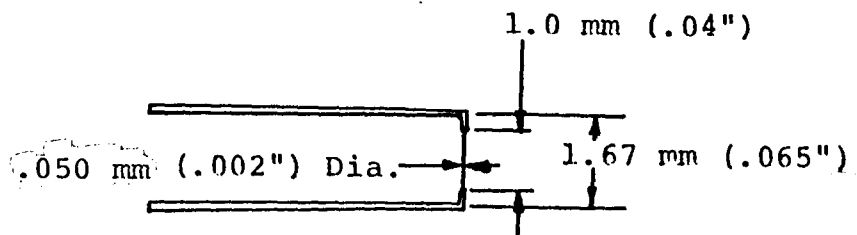
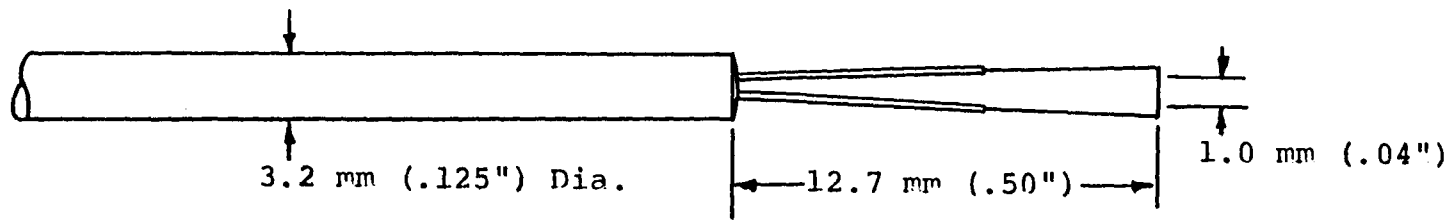
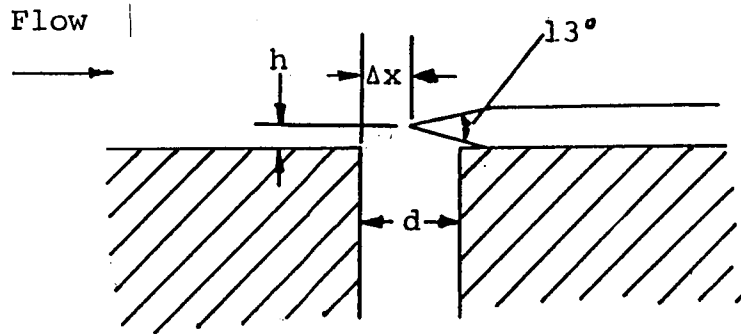


Figure 3 - Four Tube Probe.



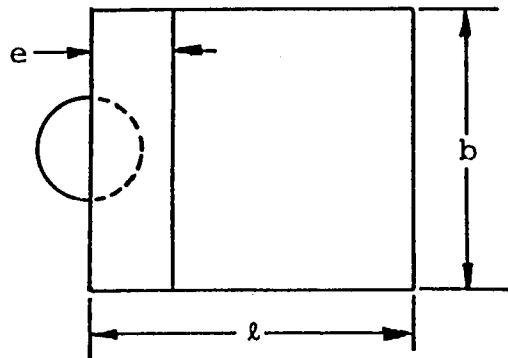
Tip Detail

Figure 4 - Hot Film Probe.



Surface Static Pressure Tap

Dimensions	
d	1.07 mm (.042")
e	.46 mm (.018")
h	.05 mm (.002")
ℓ	6.35 mm (.25")
b	6.35 mm (.25")
d/h	20.5
b/h	122.0
ℓ/b	1.0
Δx	0.0



Criteria from Ref.7:

$$\frac{d}{h} > 6$$

$$\frac{b}{h} > 36$$

$$\frac{\ell}{b} = 1$$

$$\Delta x = 0$$

Figure 5 - Razor Blade Technique: Details of Dimensions and Positioning.

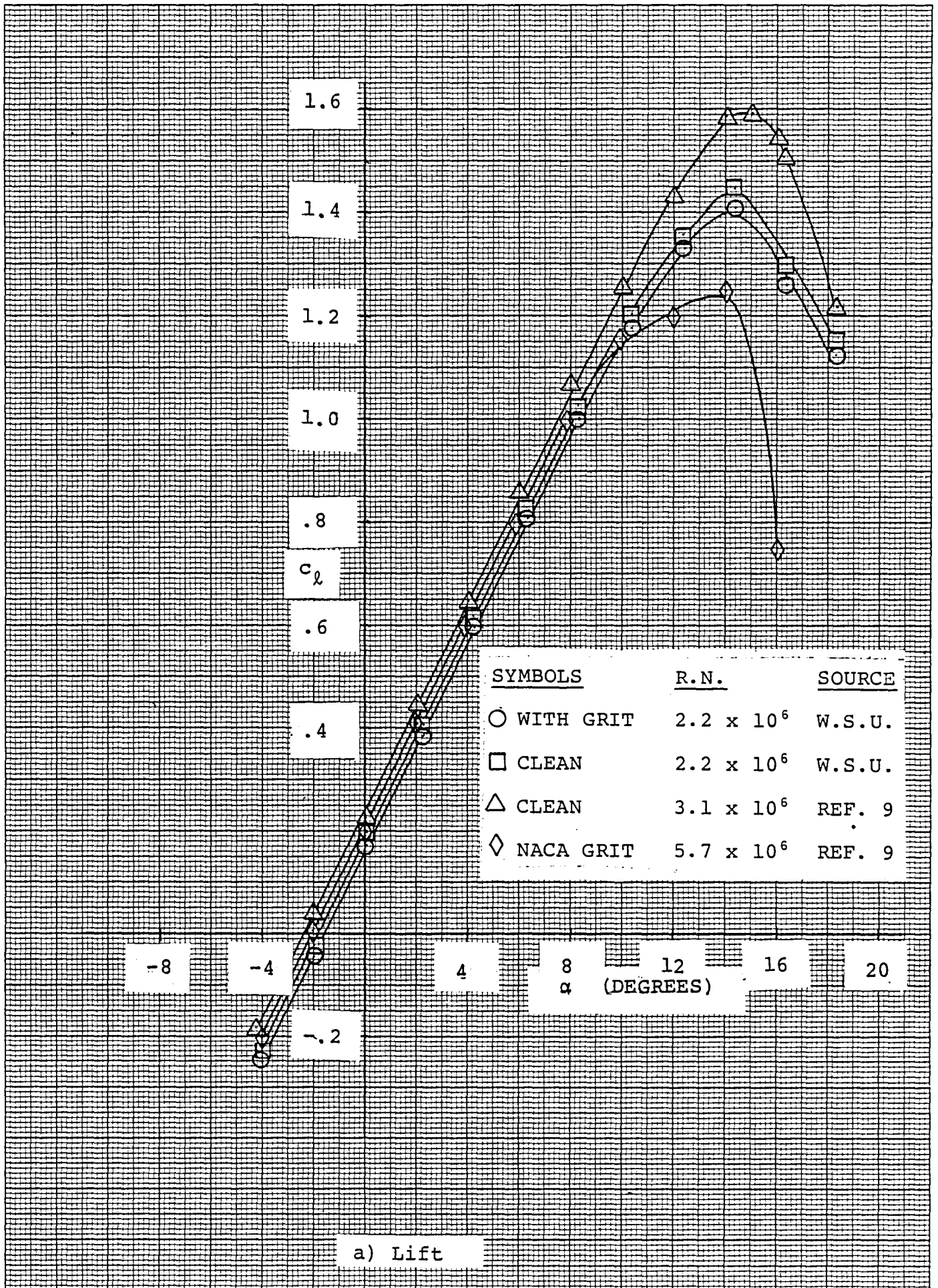
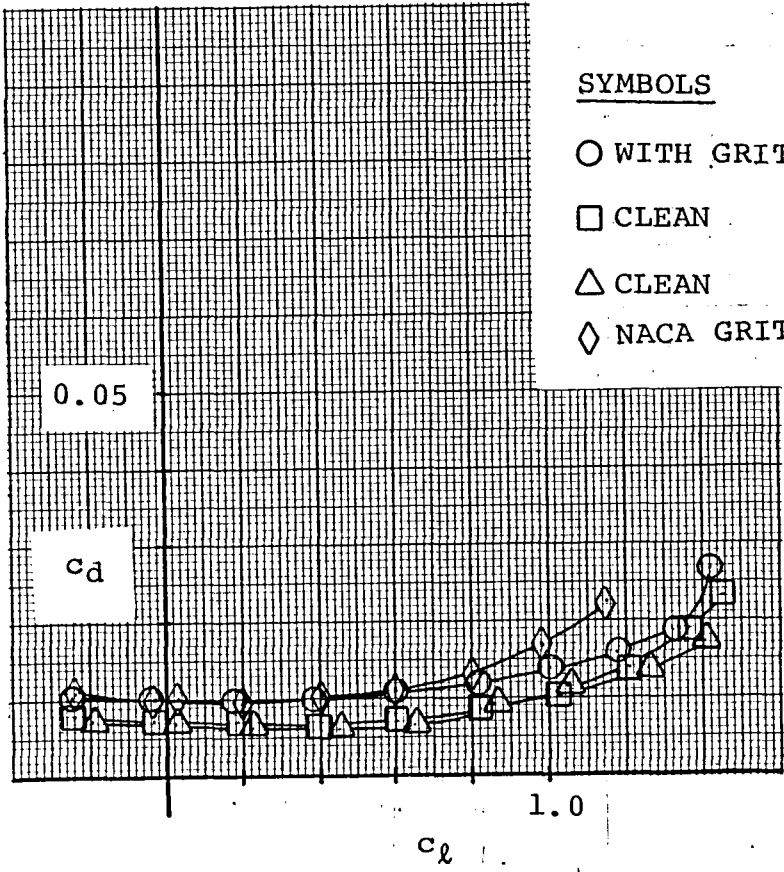
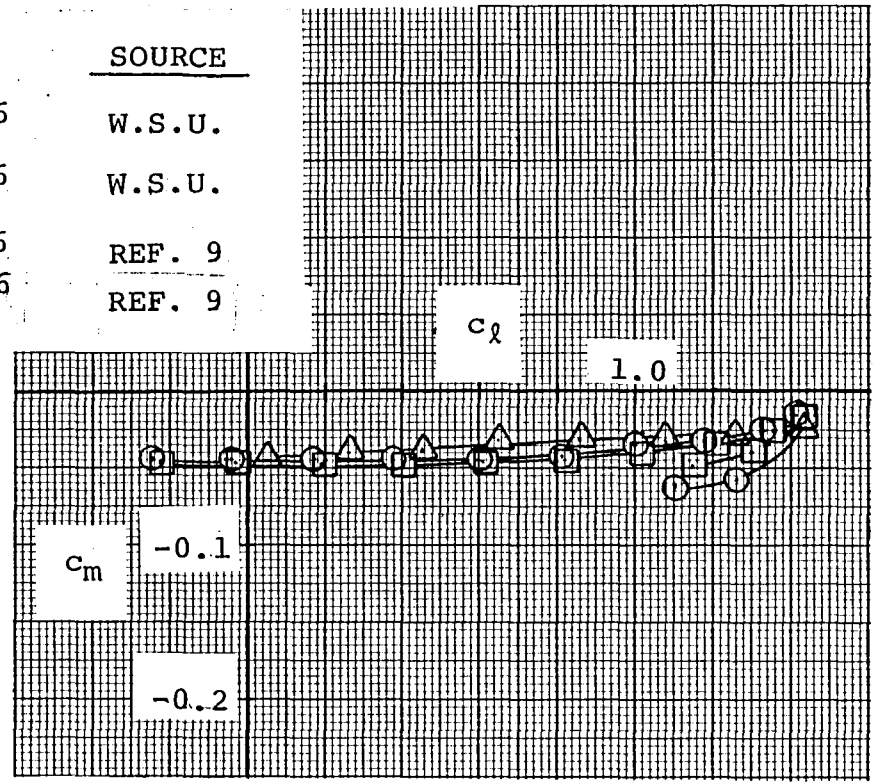


Figure 6 - Aerodynamic Coefficient Variation of 2412 Airfoil.



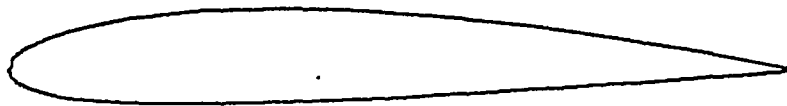
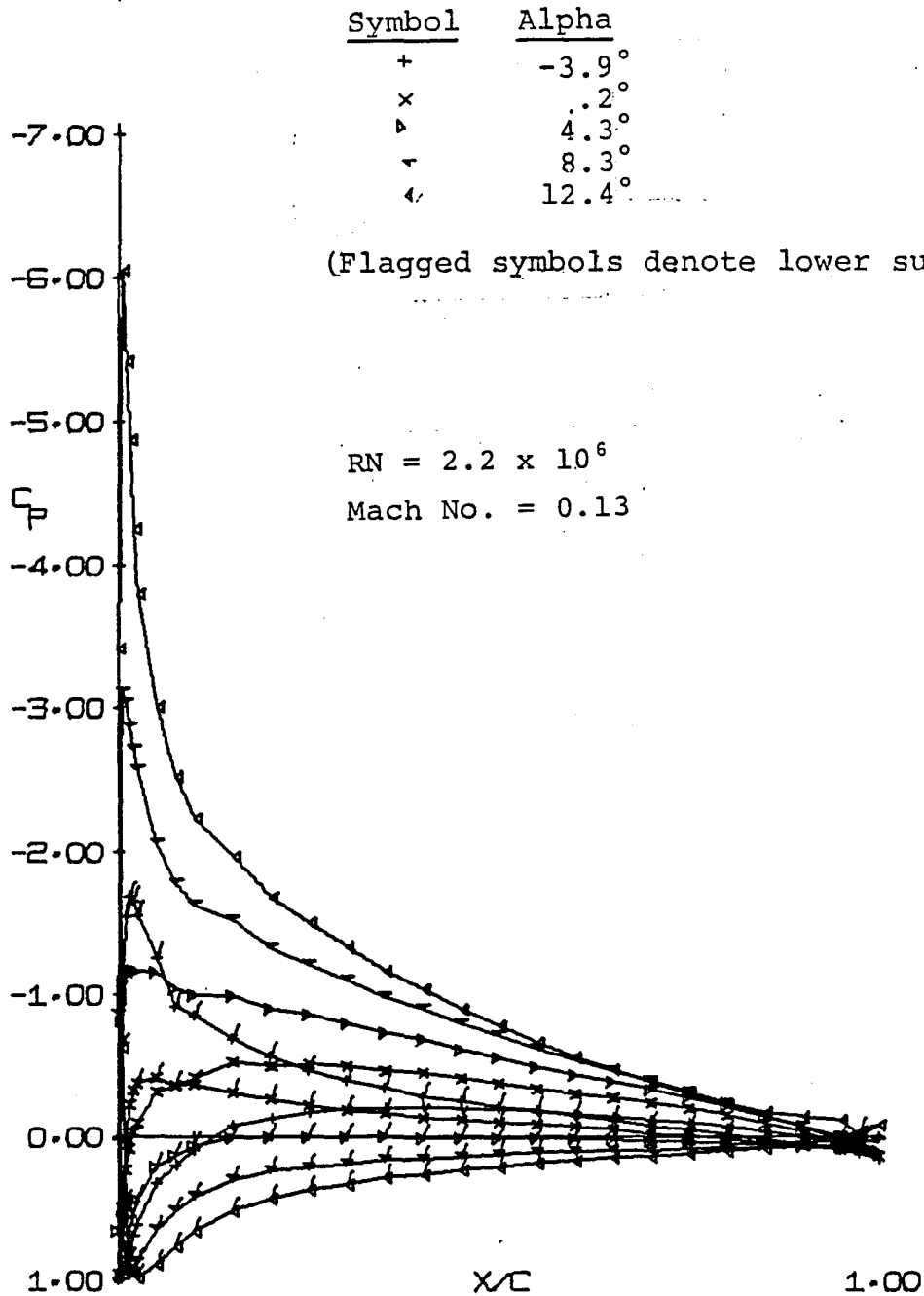
b) Drag

SYMBOLS	R.N.	SOURCE
○ WITH GRIT	$2.2 \times 10^6$	W.S.U.
□ CLEAN	$2.2 \times 10^6$	W.S.U.
△ CLEAN	$3.1 \times 10^6$	REF. 9
◇ NACA GRIT	$5.7 \times 10^6$	REF. 9



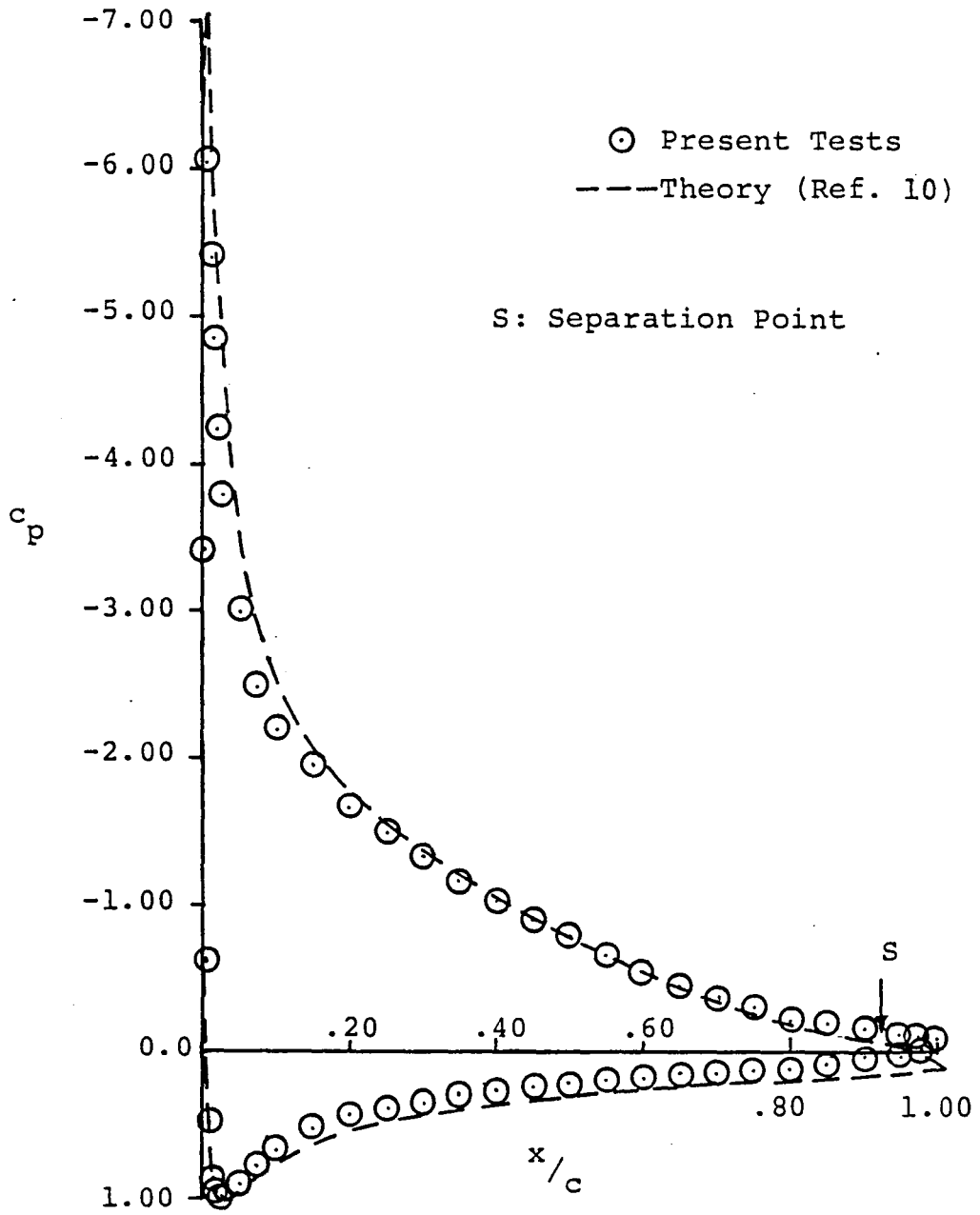
c) Pitching Moment

Figure 6 - Concluded.



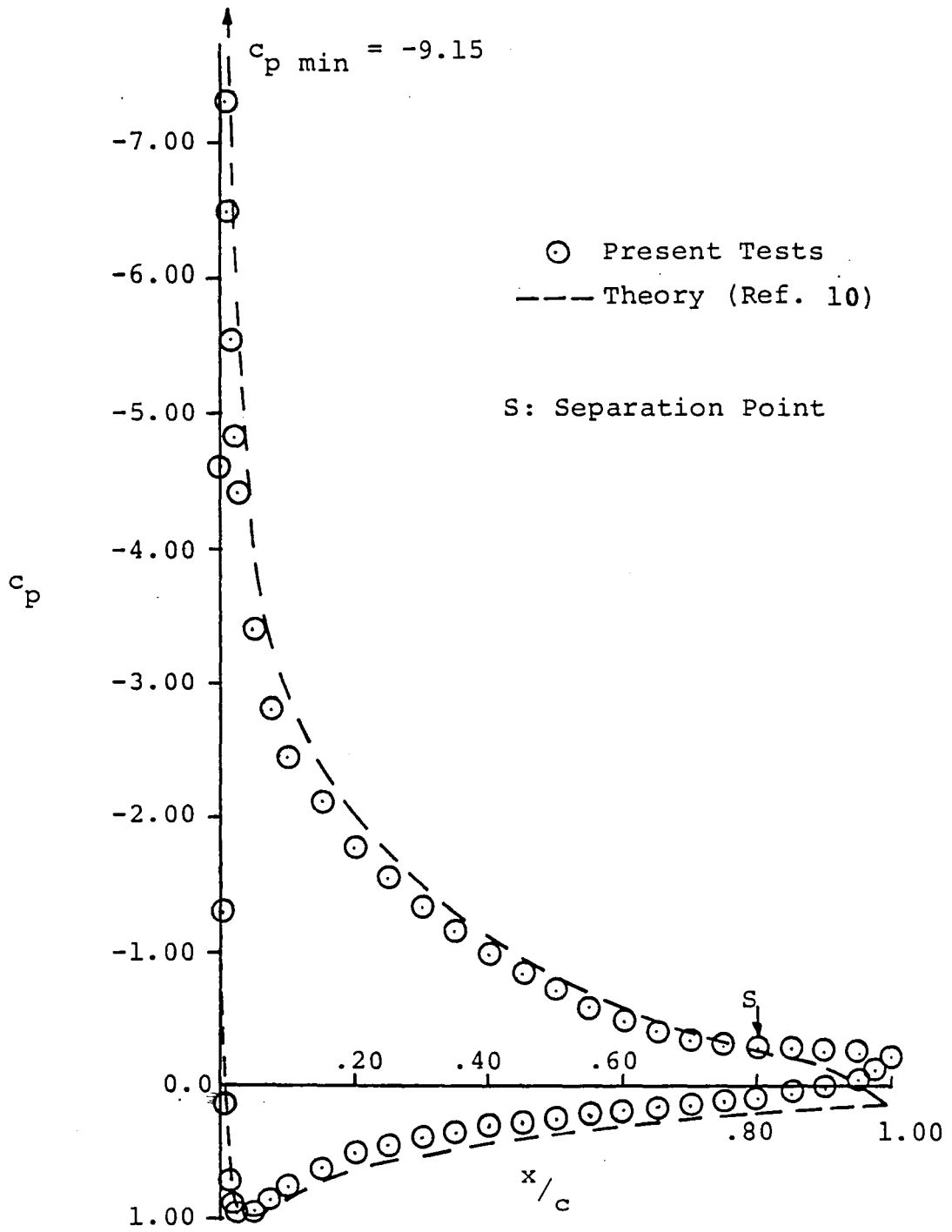
a) Pre-stall angles of attack

Figure 7 - Pressure Distributions of 2412 Airfoil.



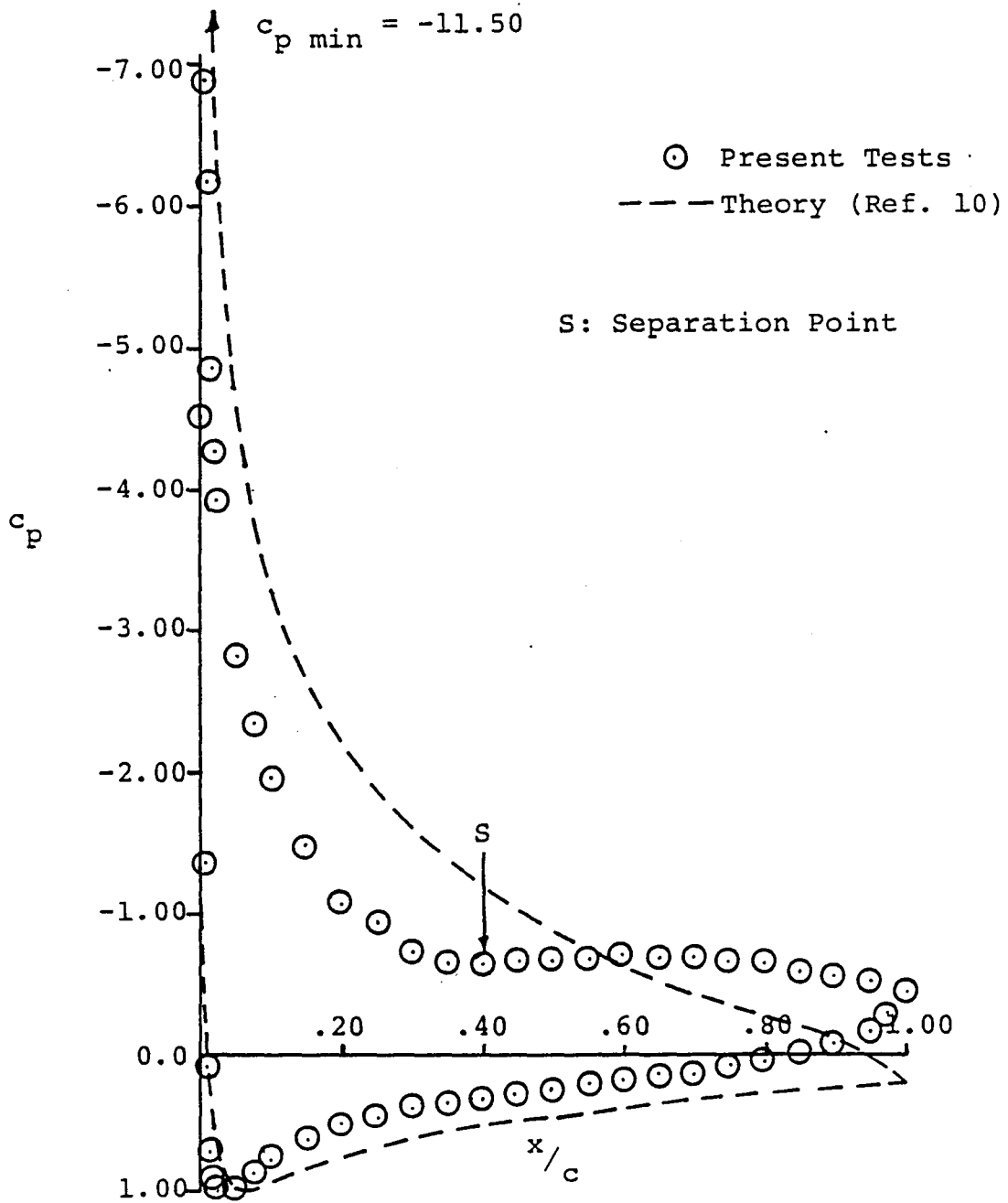
b) Pre-stall angle of attack,  $\alpha=12.4^\circ$

Figure 7 - Continued.



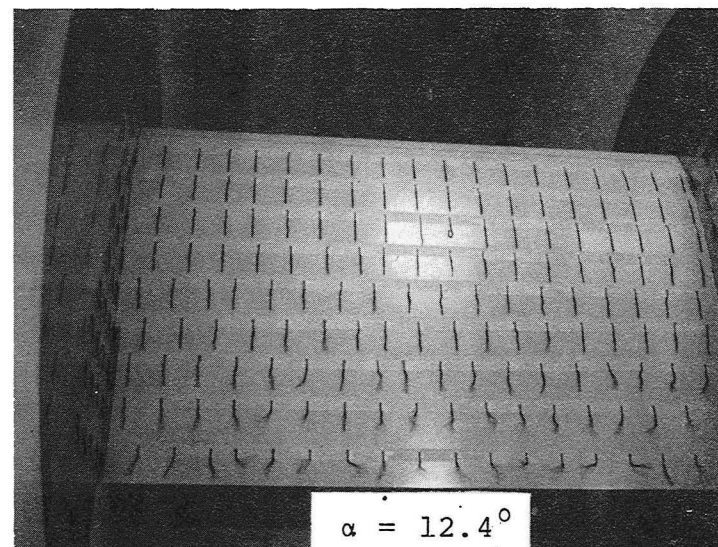
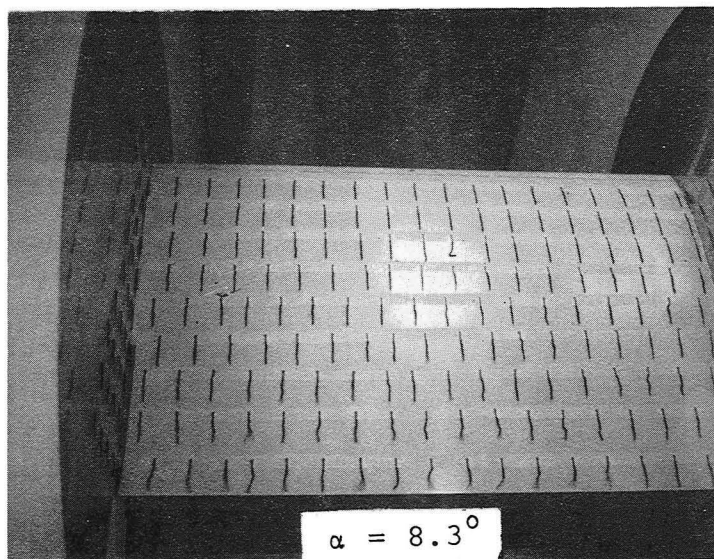
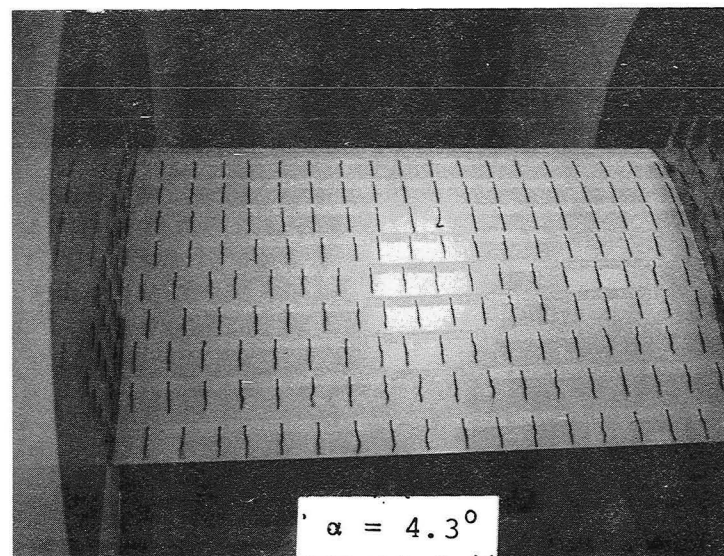
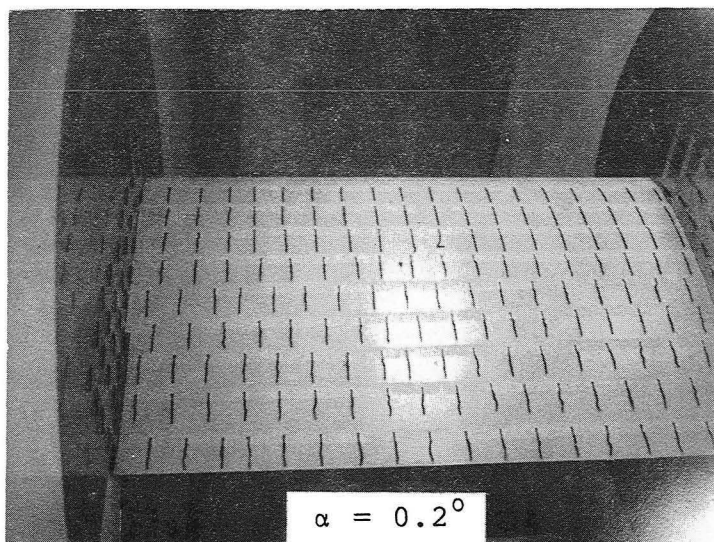
c) Stall angle of attack,  $\alpha=14.4^\circ$

Figure 7 - Continued.



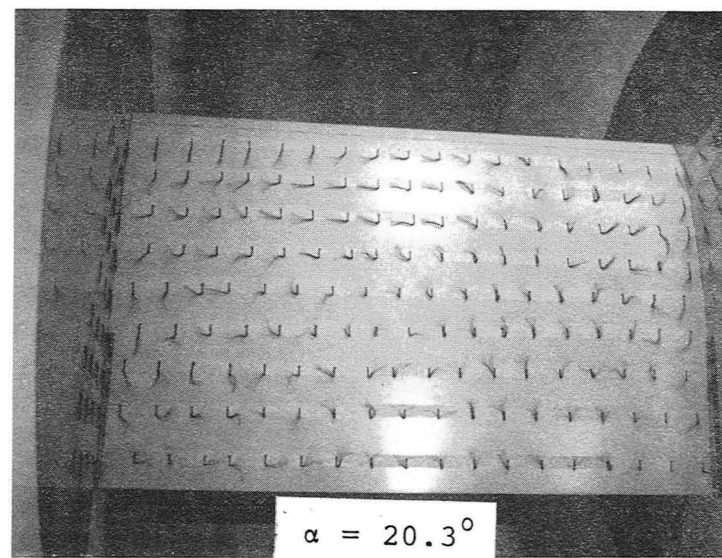
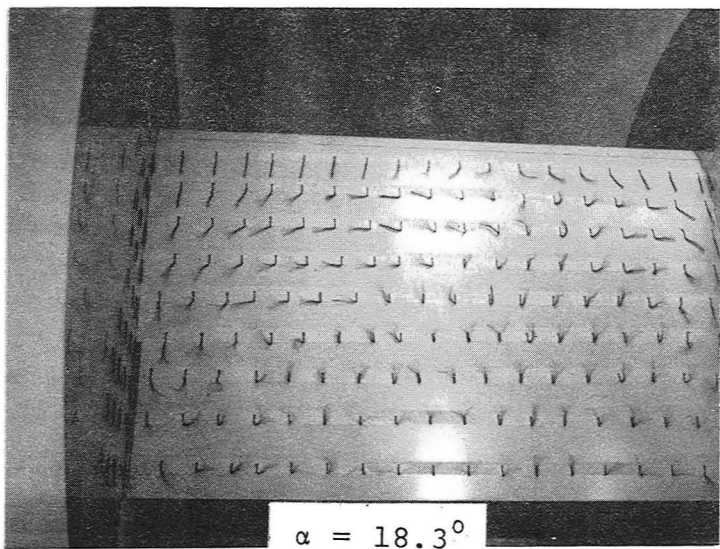
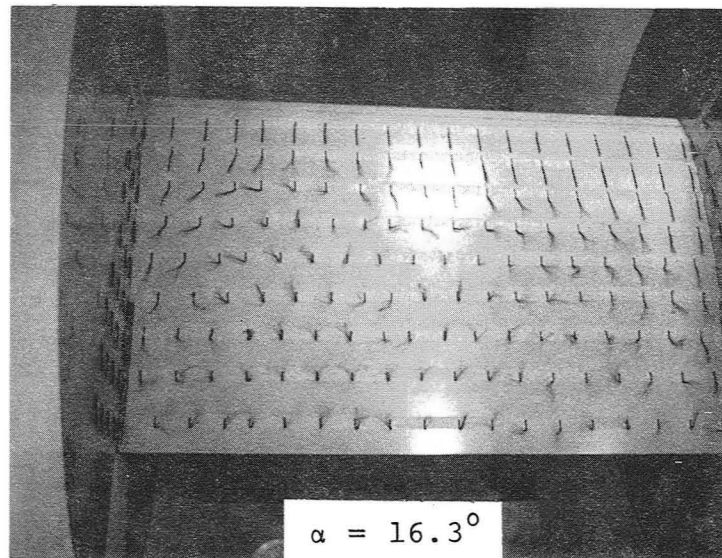
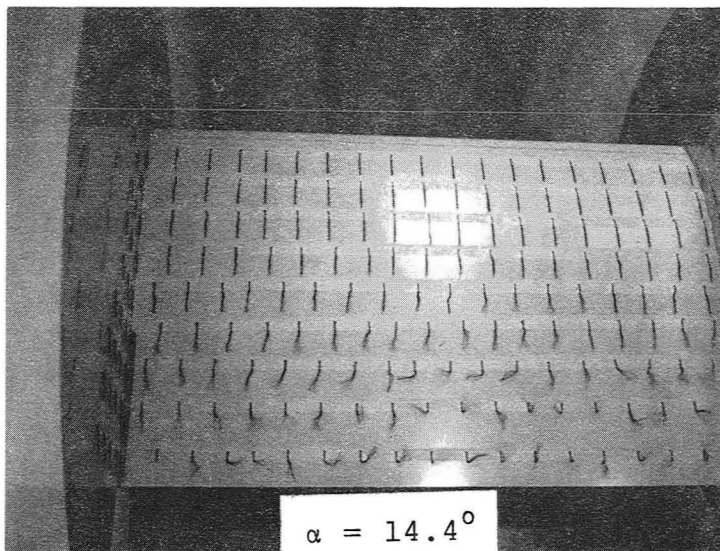
d) Post-stall angle of attack,  $\alpha=16.4^\circ$

Figure 7 - Concluded.



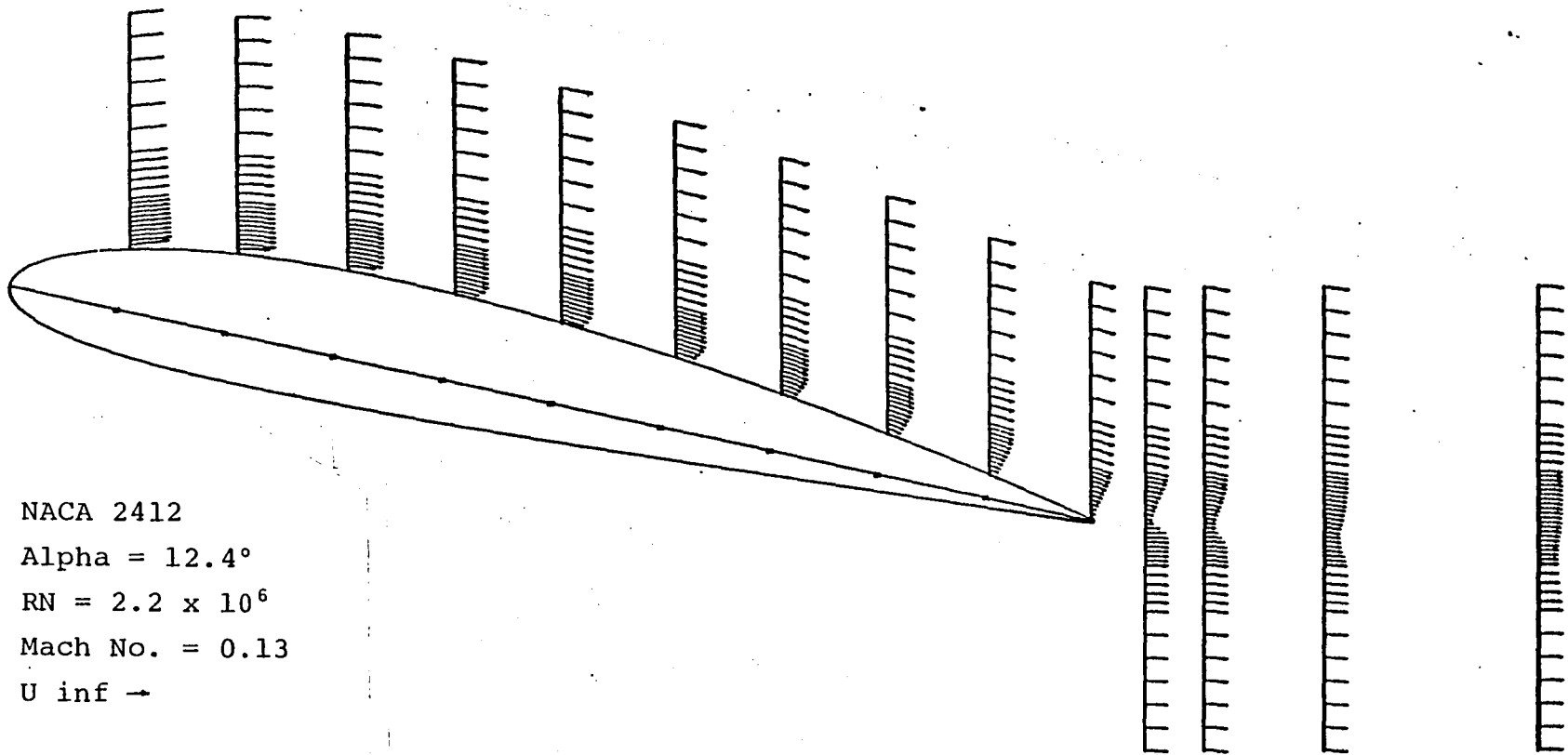
a) Pre-stall angles of attack

Figure 8 - Tuft Studies.



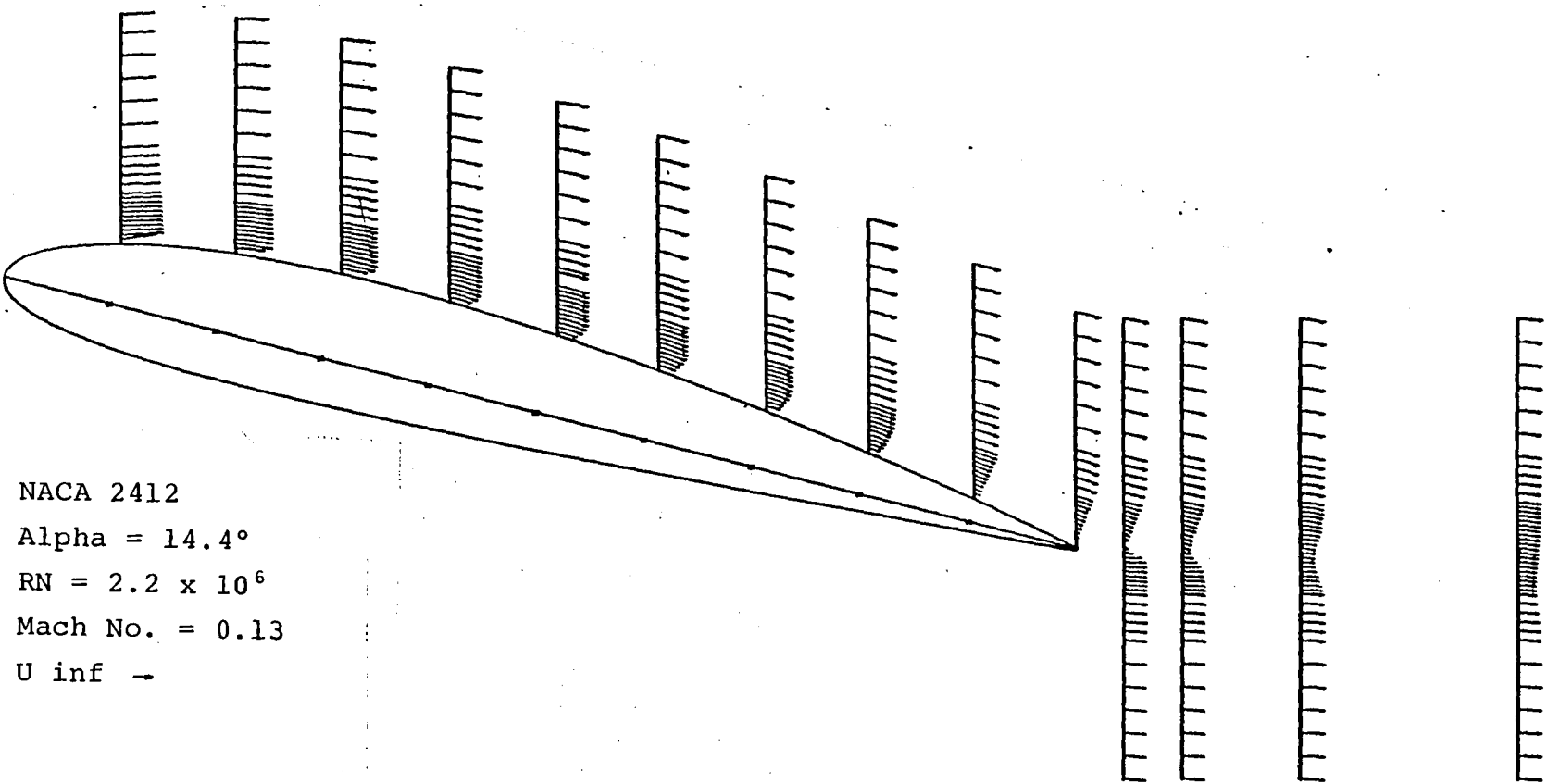
b) Stall and post-stall angles of attack

Figure 8 - Concluded.



a) Pre-stall angle of attack,  $\alpha=12.4^\circ$

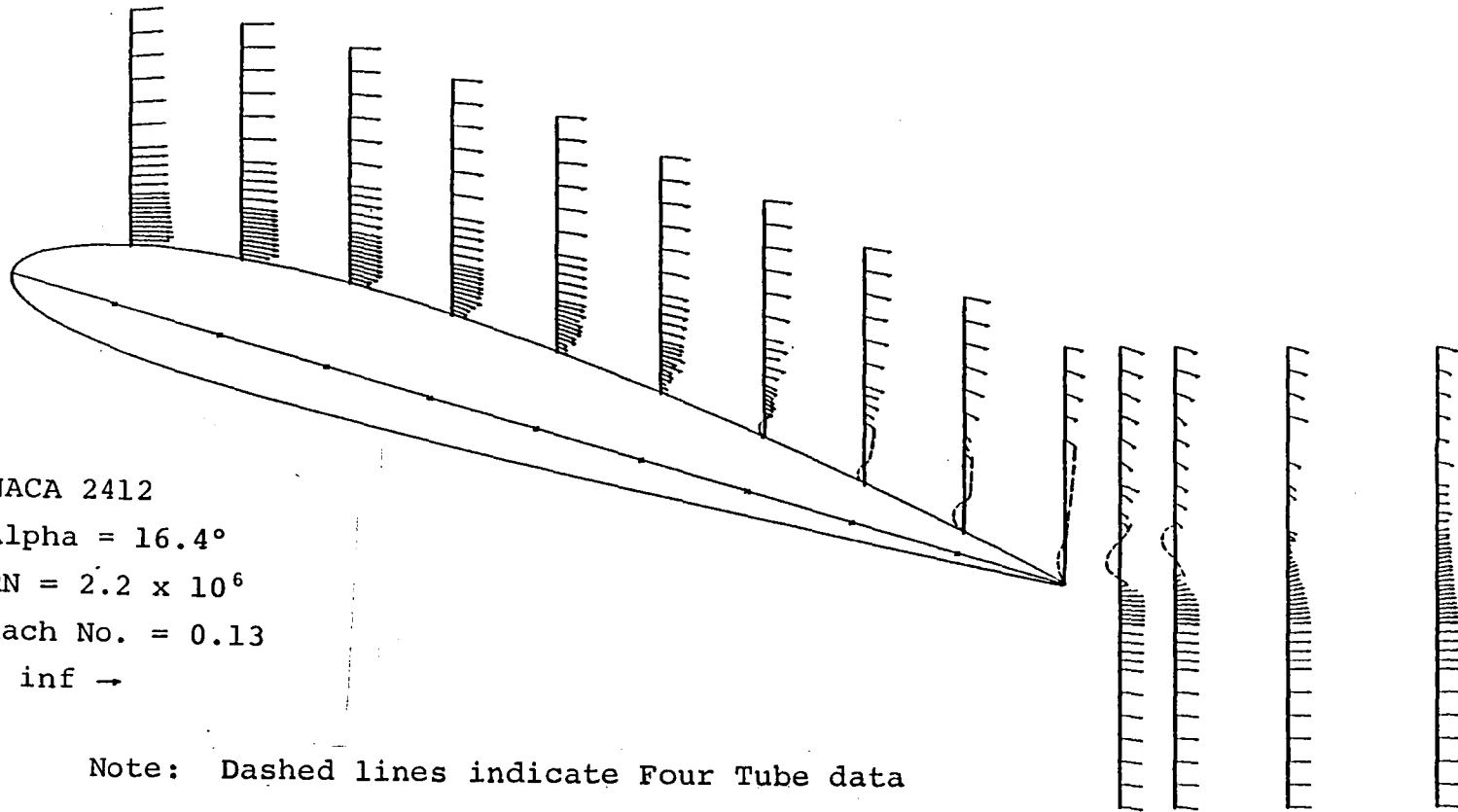
Figure 9 - Experimental Velocity Profiles.



NACA 2412  
 Alpha = 14.4°  
 RN = 2.2 x 10<sup>6</sup>  
 Mach No. = 0.13  
 U inf ↓

b) Stall angle of attack,  $\alpha=14.4^\circ$

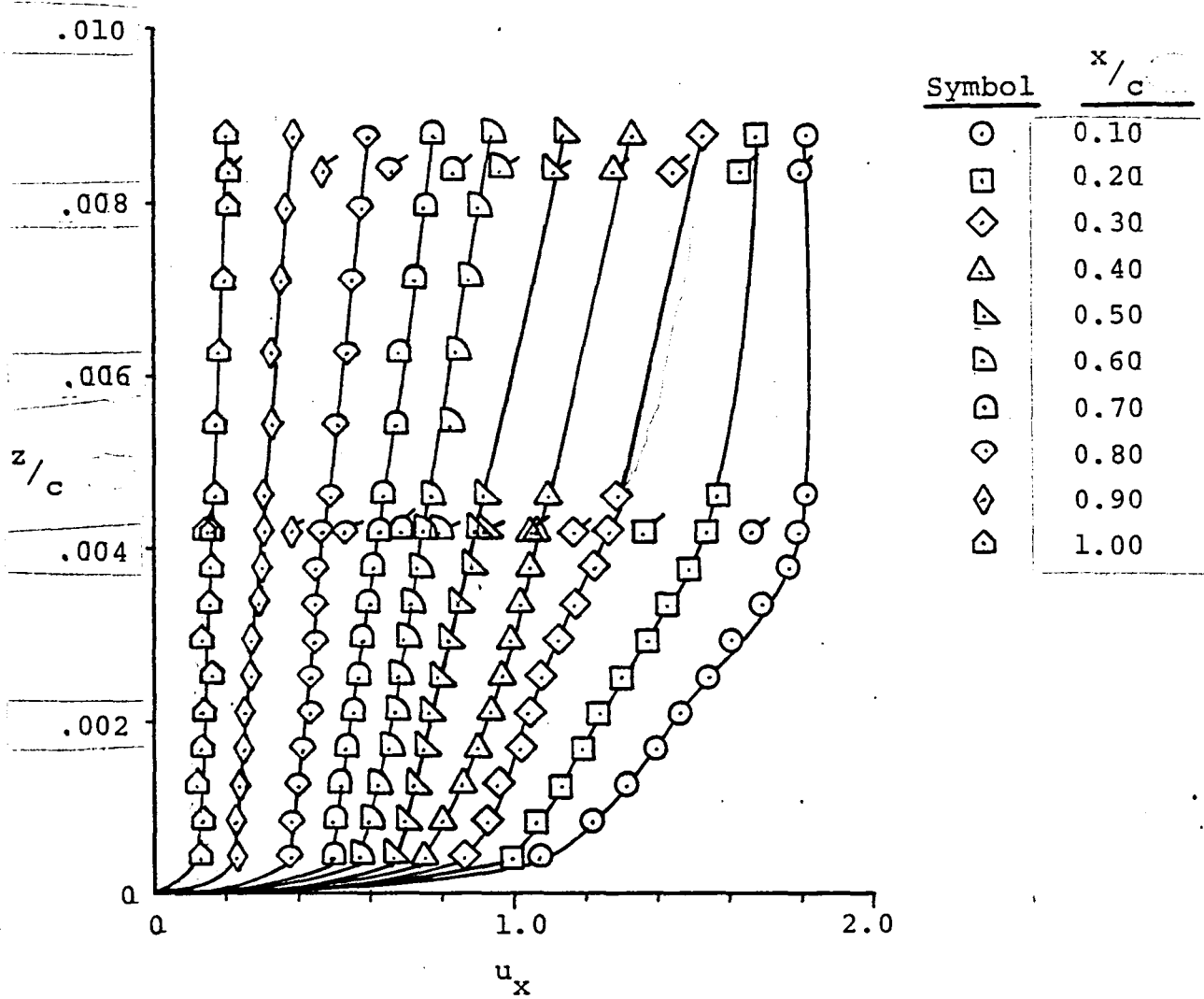
Figure 9 - Continued.



c) Post-stall angle of attack,  $\alpha=16.4^\circ$

Figure 9 - Concluded.

Primed: Five Tube Probe  
 Unprimed: Four Tube Probe

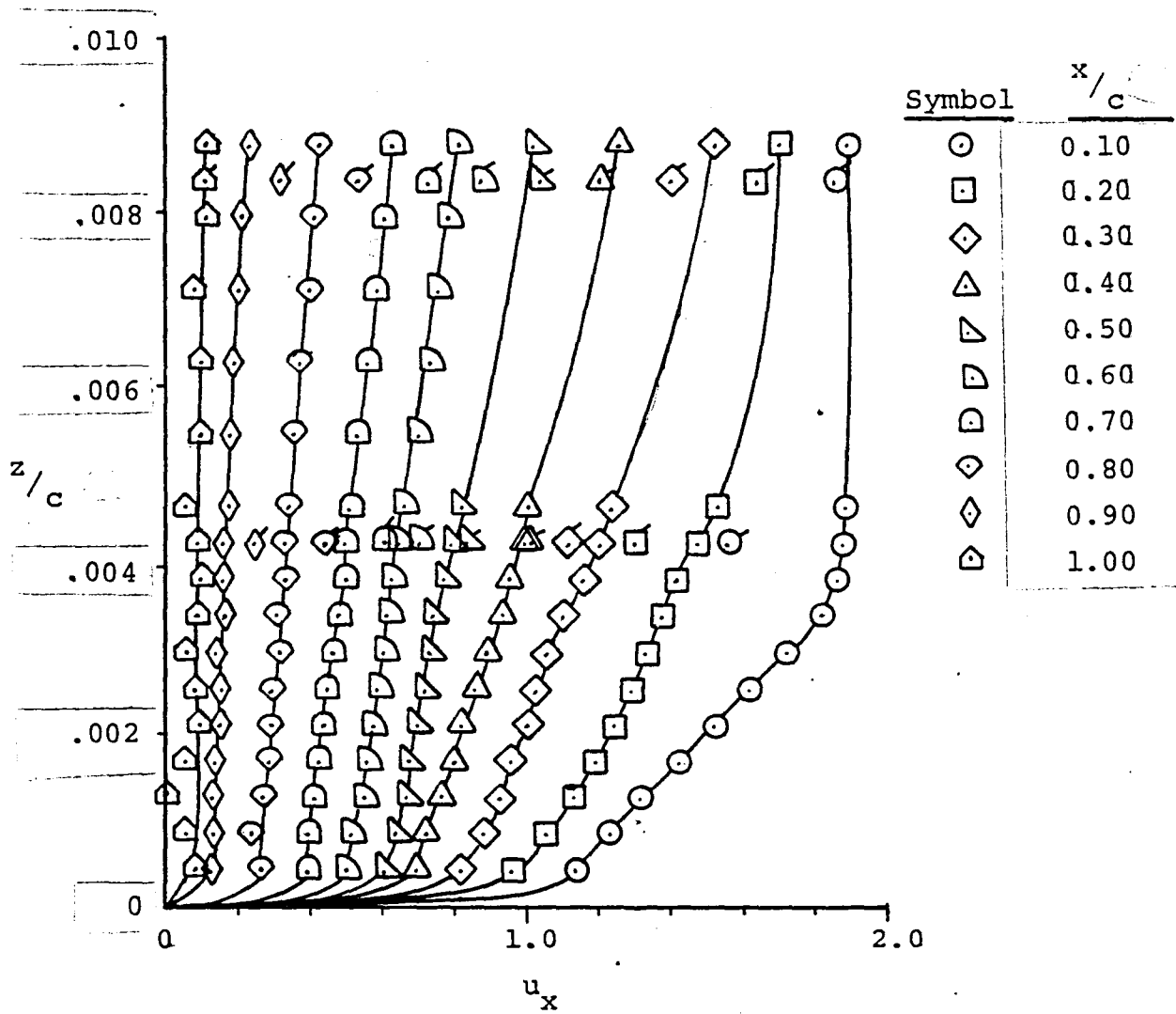


a) Pre-stall angle of attack,  $\alpha=12.4^\circ$

Figure 10 - Near Wall Velocity Profiles.

Primed: Five Tube Probe

Unprimed: Four Tube Probe

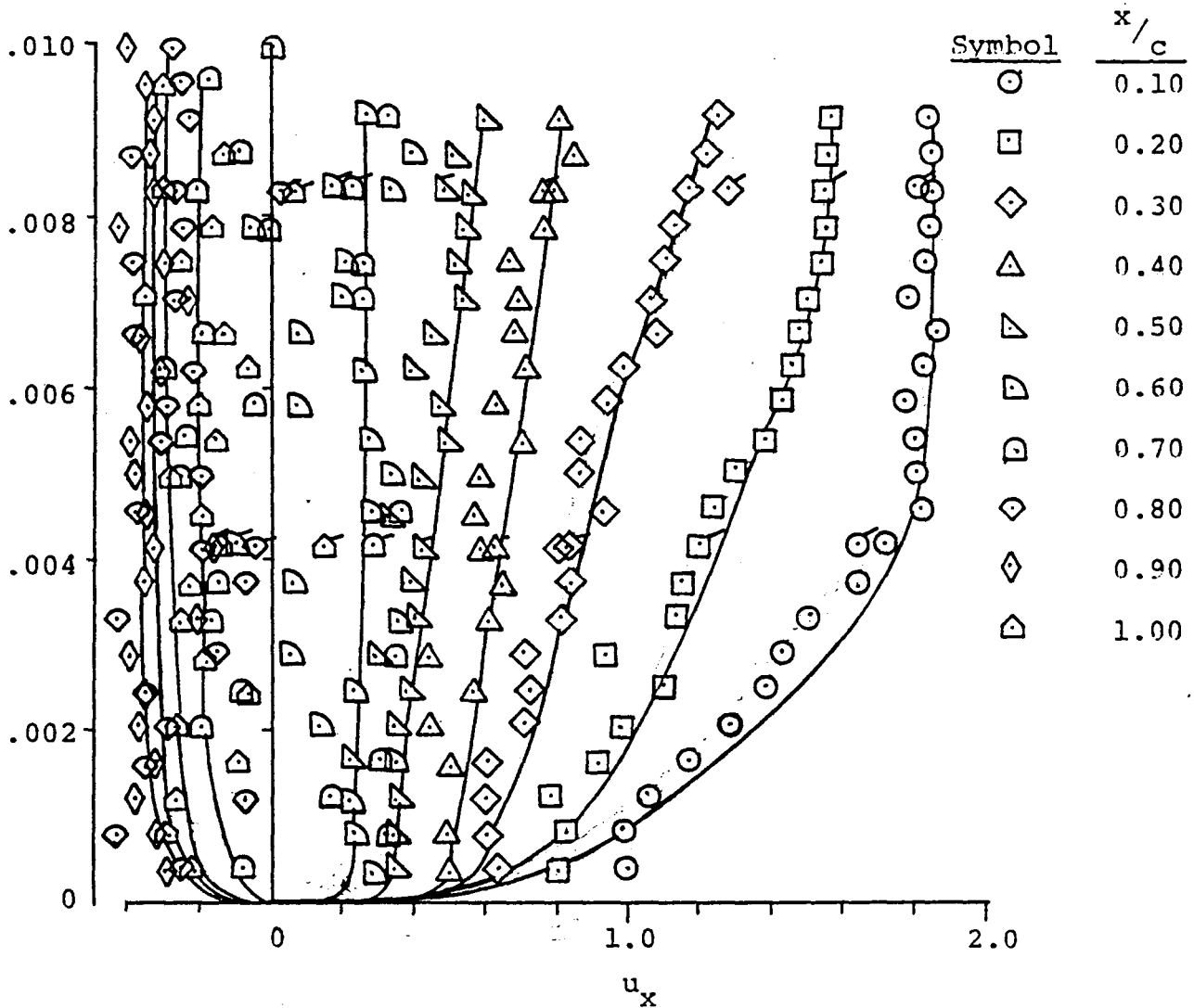


b) Stall angle of attack,  $\alpha=14.4^\circ$

Figure 10 - Continued.

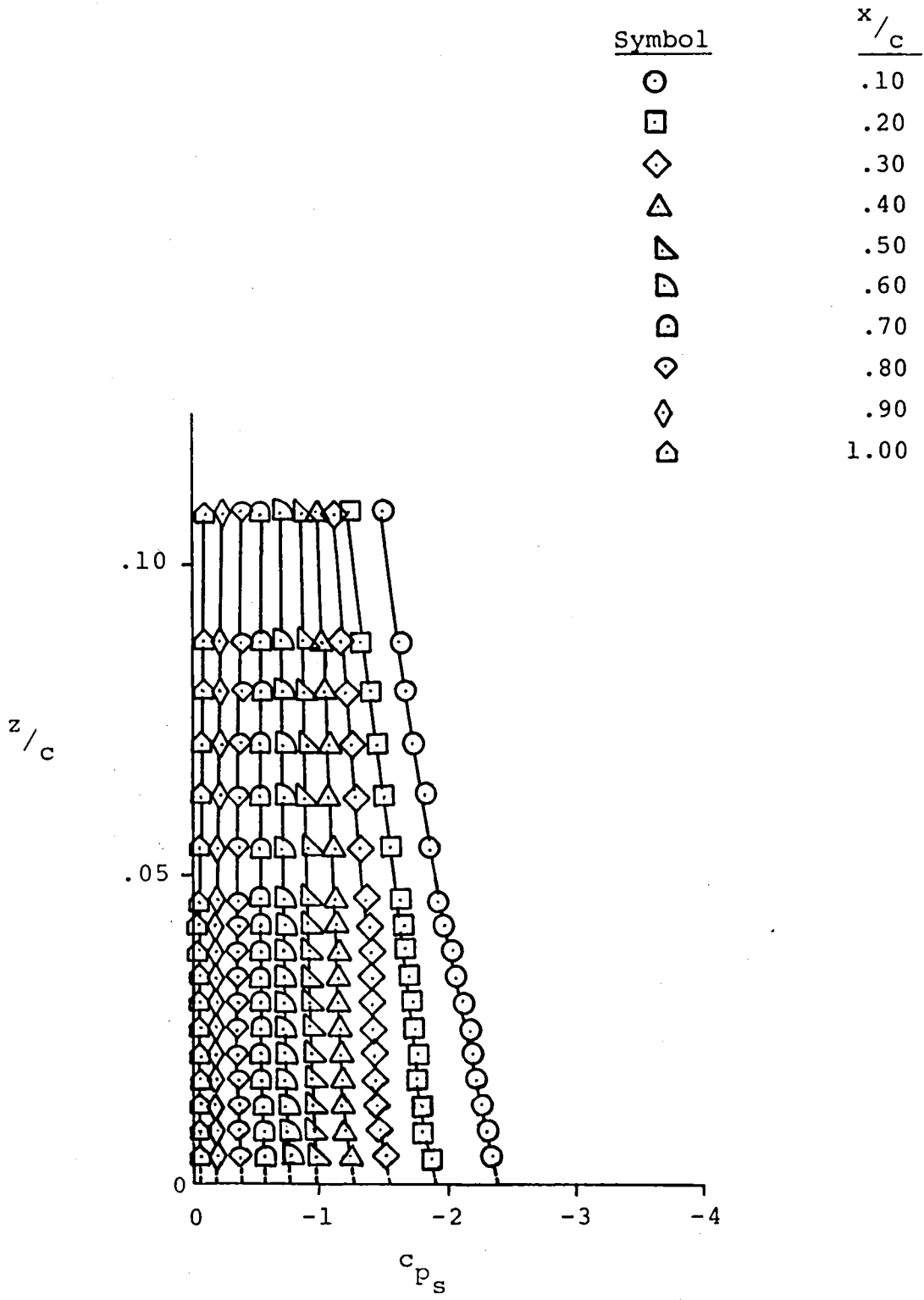
Primed: Five Tube Probe

Unprimed: Four Tube Probe



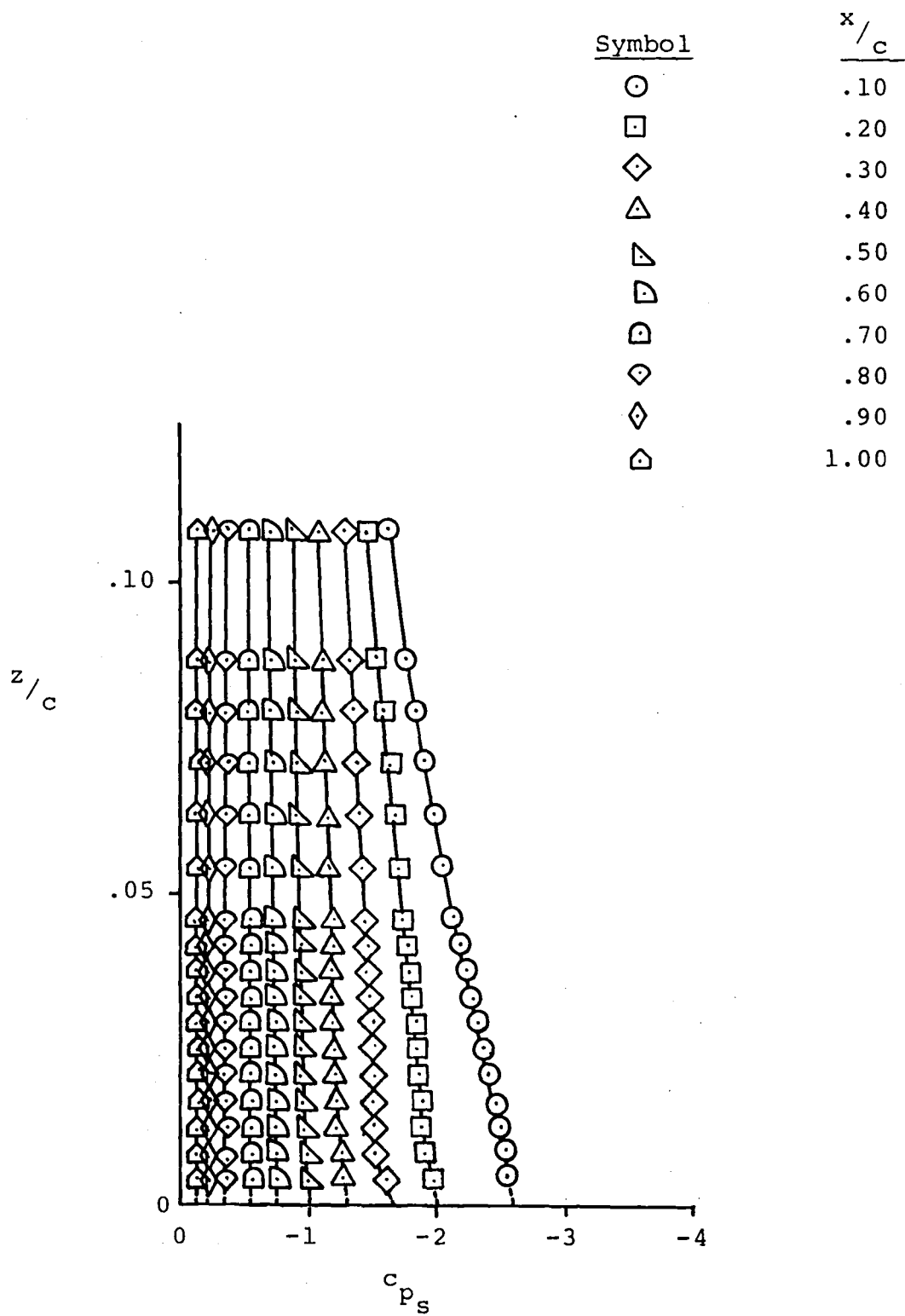
c) Post-stall angle of attack,  $\alpha = 16.4^\circ$

Figure 10 - Concluded.



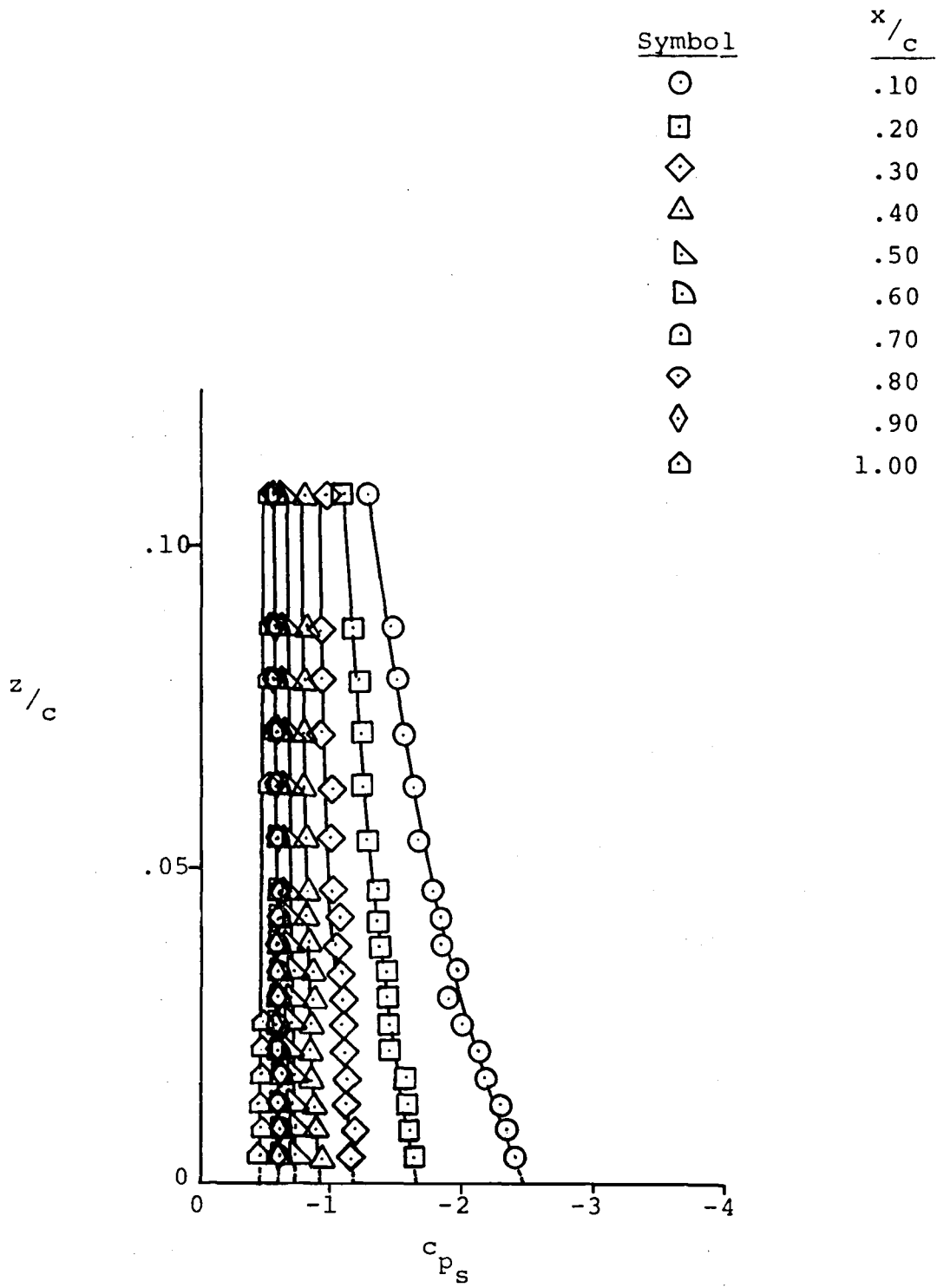
a) Pre-stall angle of attack,  $\alpha=12.4^\circ$

Figure 11 - Static Pressure Profiles.



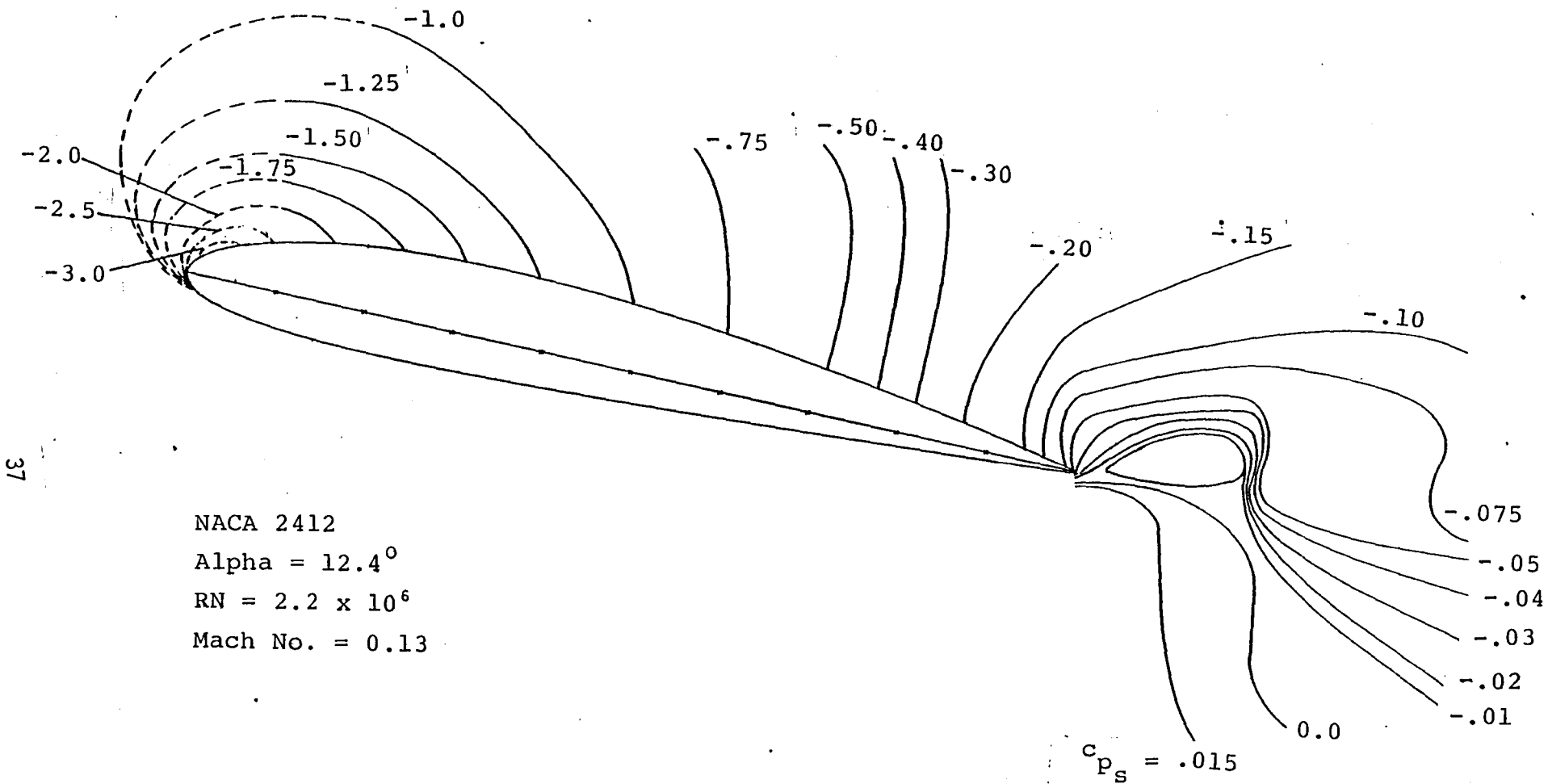
b) Stall angle of attack,  $\alpha=14.4^\circ$

Figure 11 - Continued.



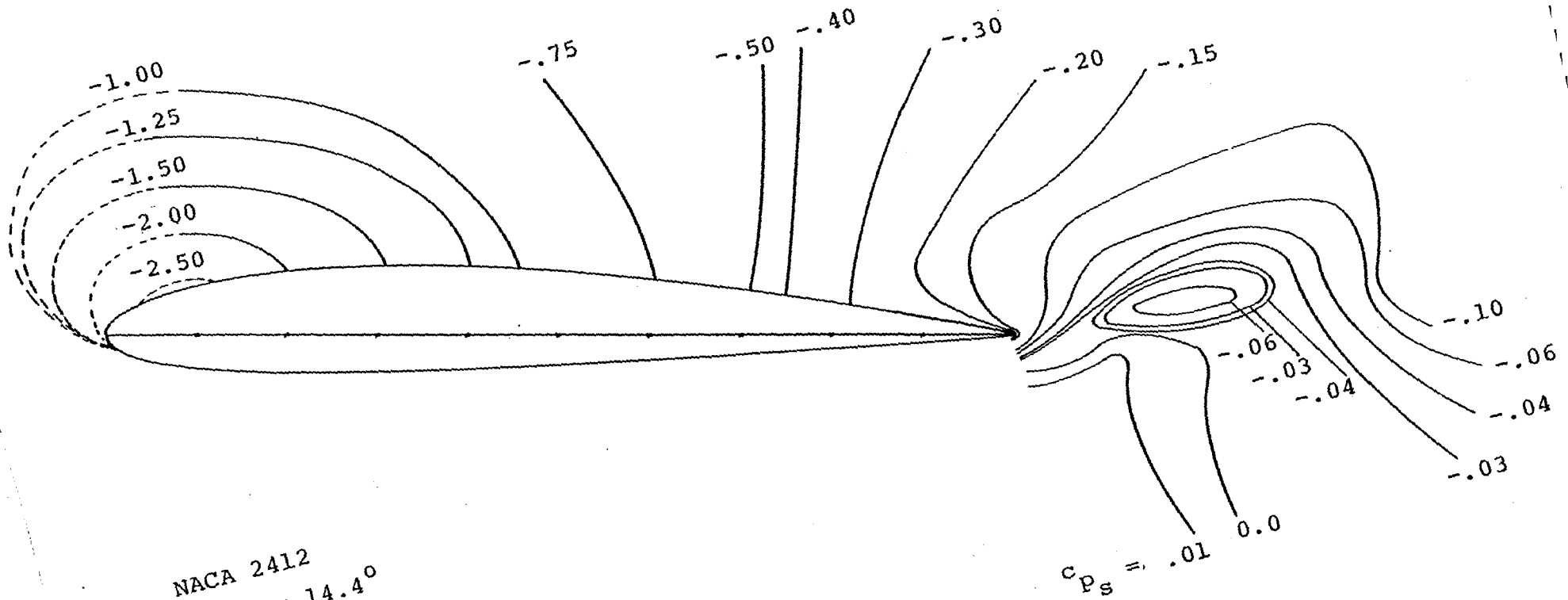
c) Post-stall angle of attack,  $\alpha=16.4^\circ$

Figure 11 - Concluded.



a) Pre-stall angle of attack,  $\alpha=12.4^\circ$

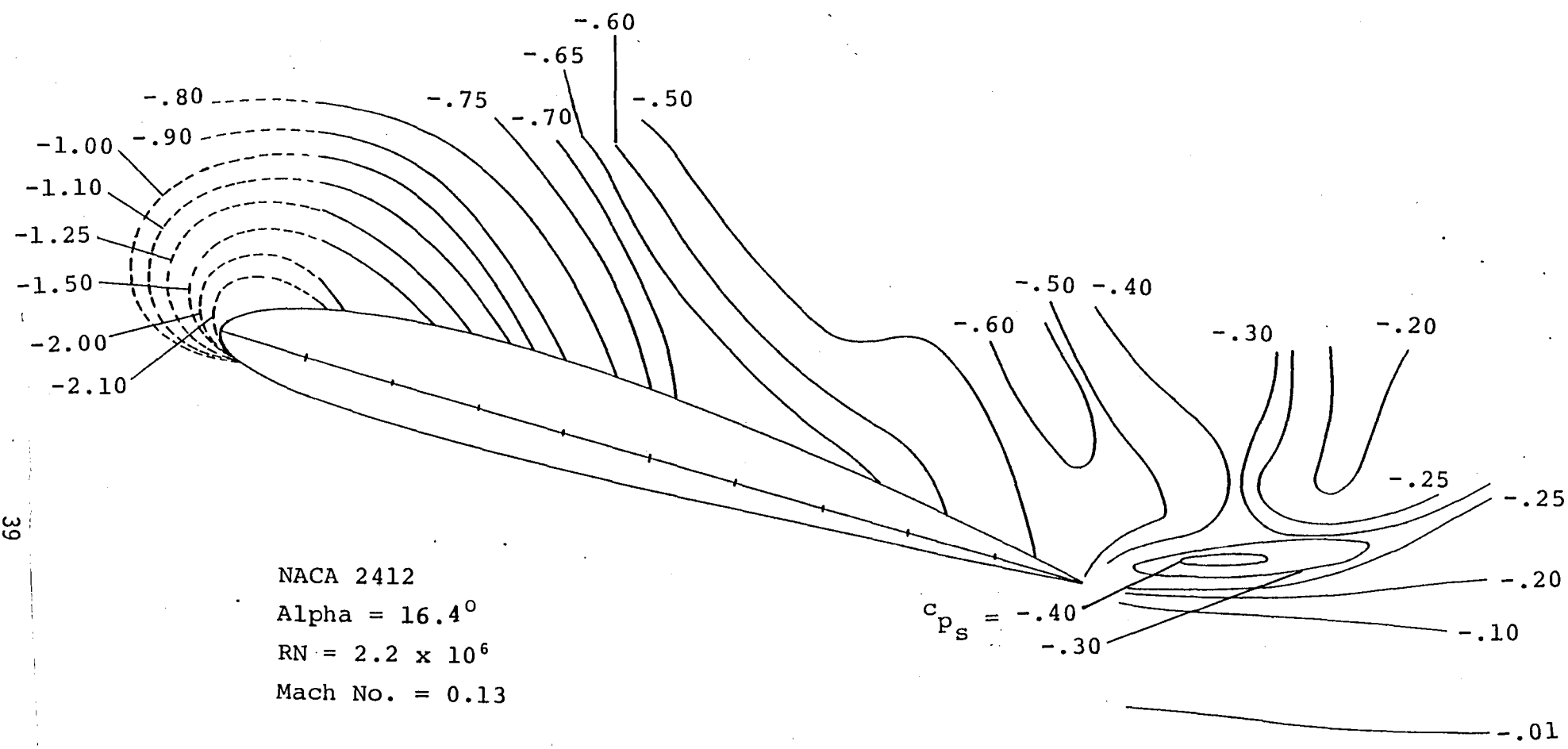
Figure 12 - Static Pressure Field Contours.



NACA 2412  
Alpha =  $14.4^\circ$   
RN =  $2.2 \times 10^6$   
Mach No. = 0.13

b) Stall angle of attack,  $\alpha=14.4^\circ$

Figure 12 - Continued.



c) Post-stall angle of attack,  $\alpha=16.4^\circ$

Figure 12 - Concluded.

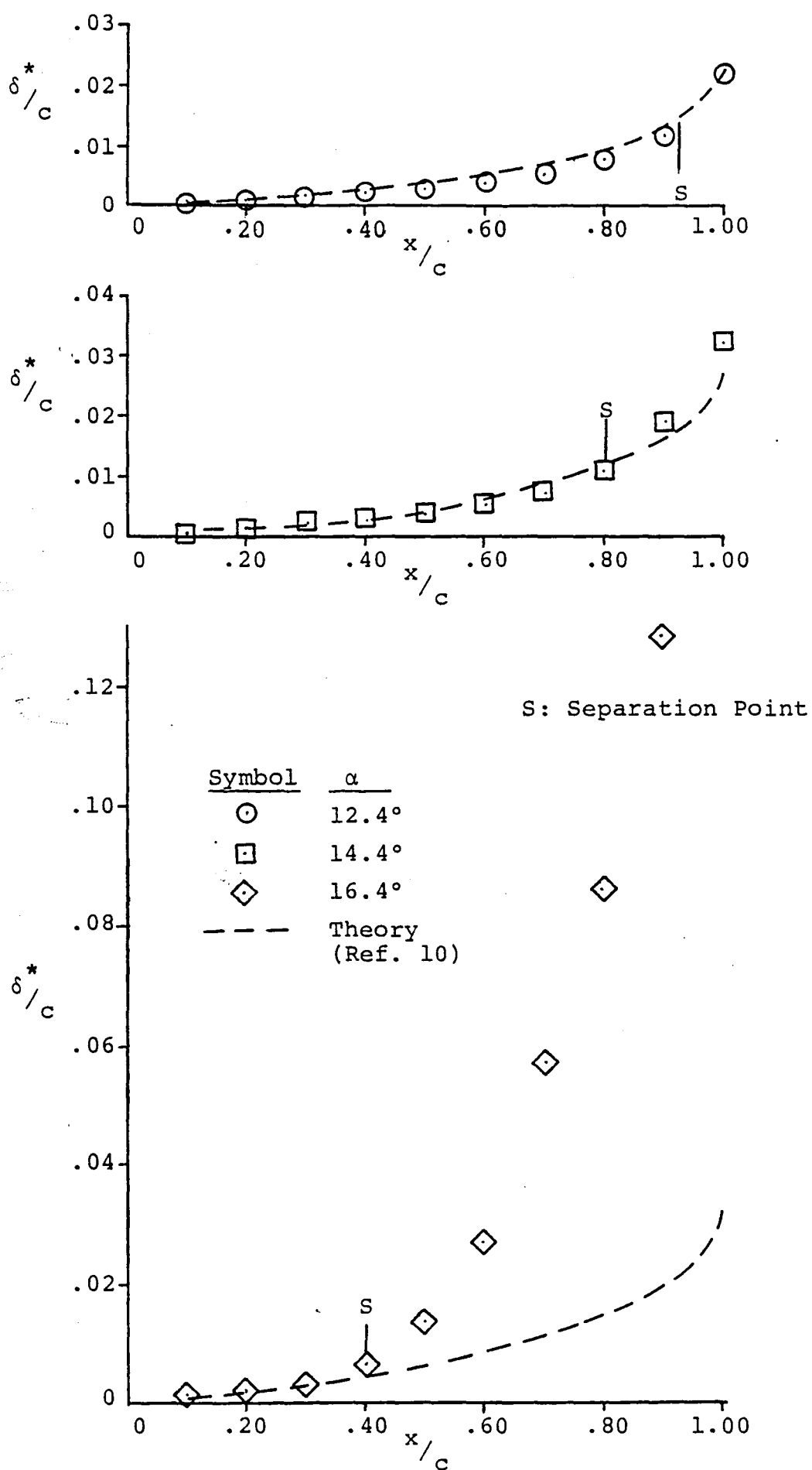


Figure 13 - Boundary Layer Displacement Thickness.

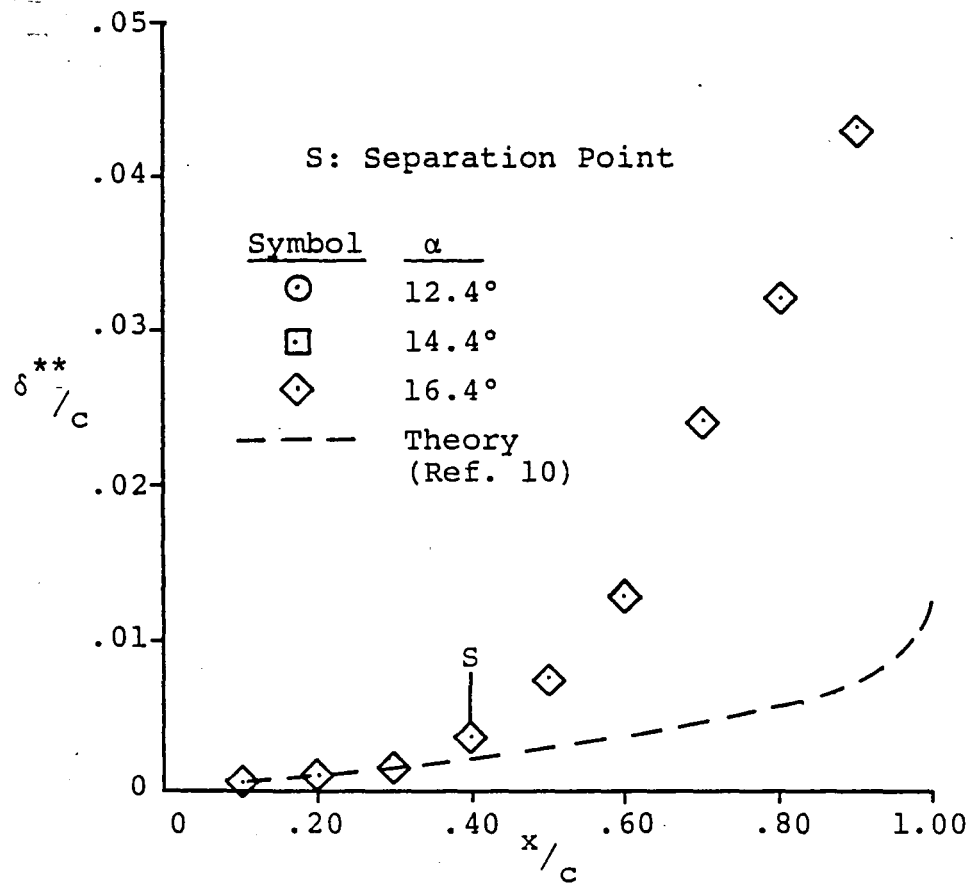
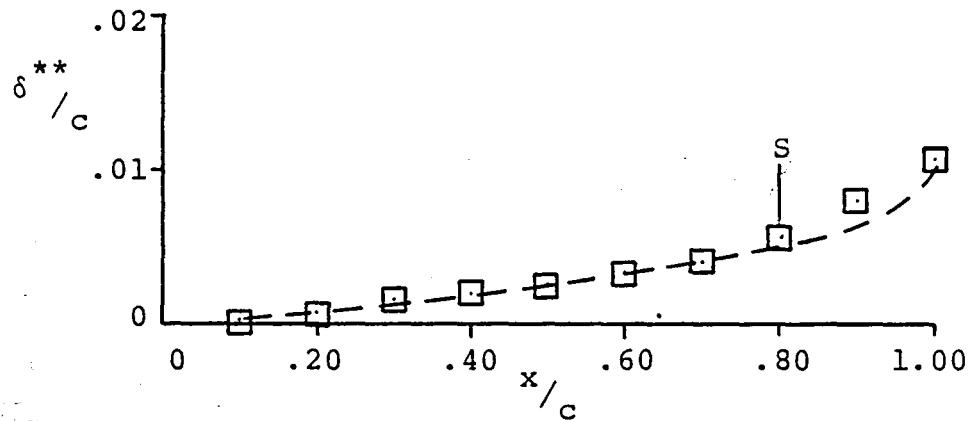
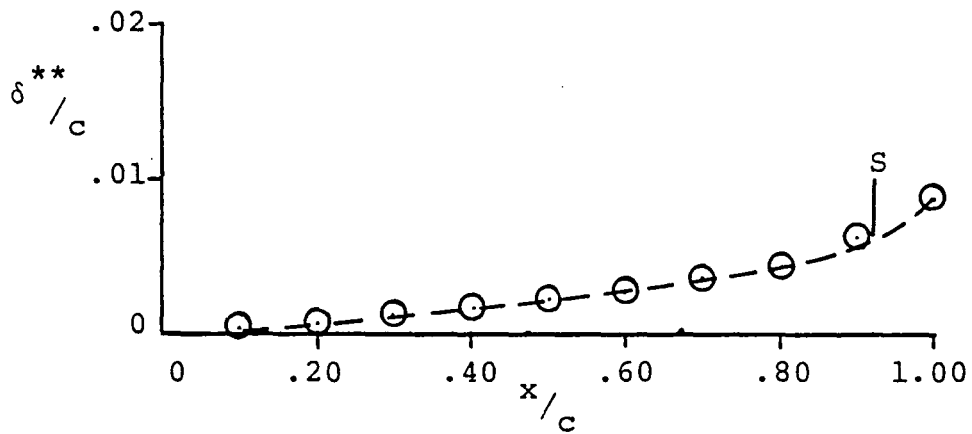


Figure 14 - Boundary Layer Momentum Thickness.

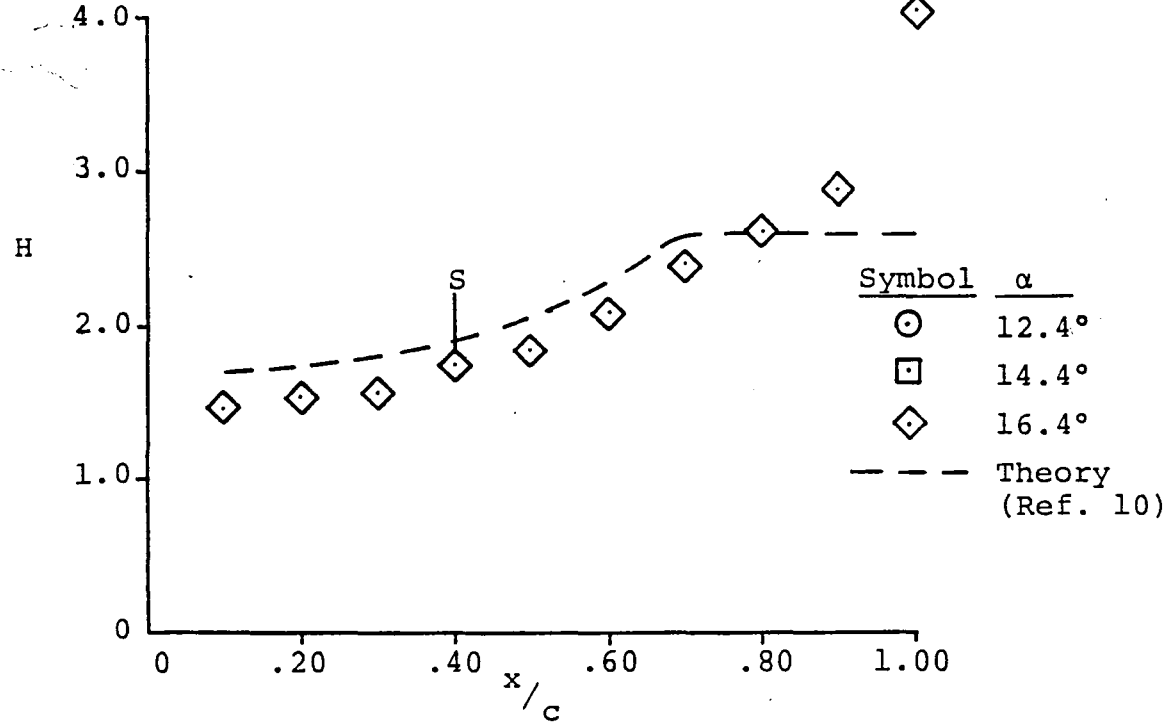
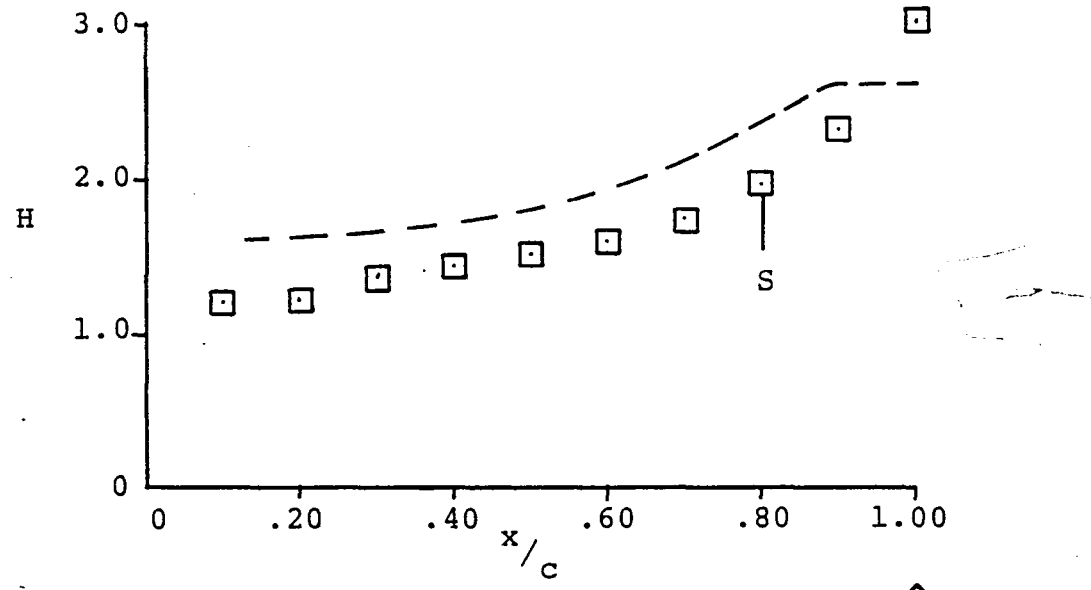
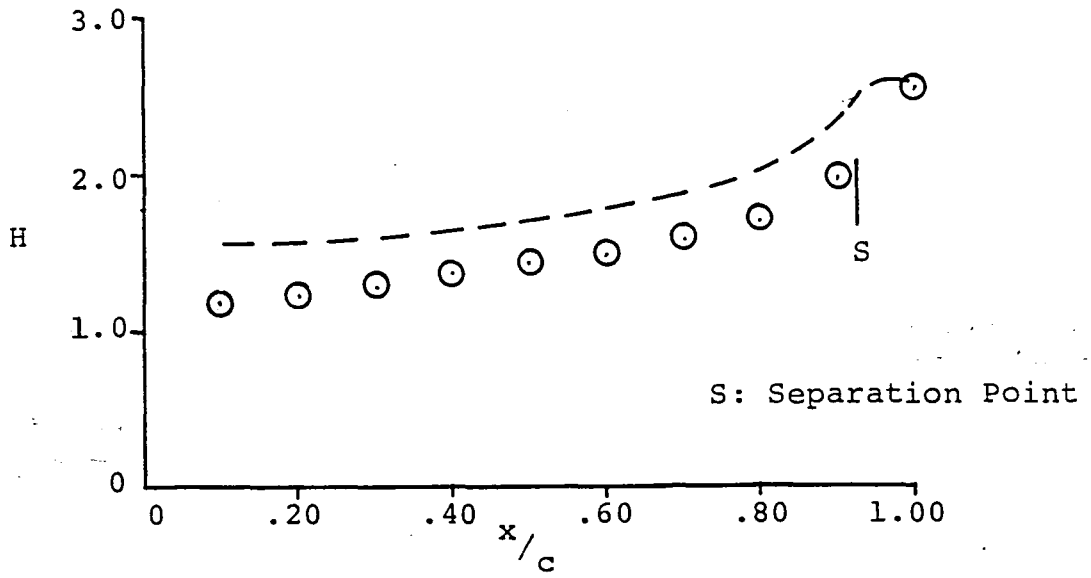


Figure 15 - Boundary Layer Shape Factor.

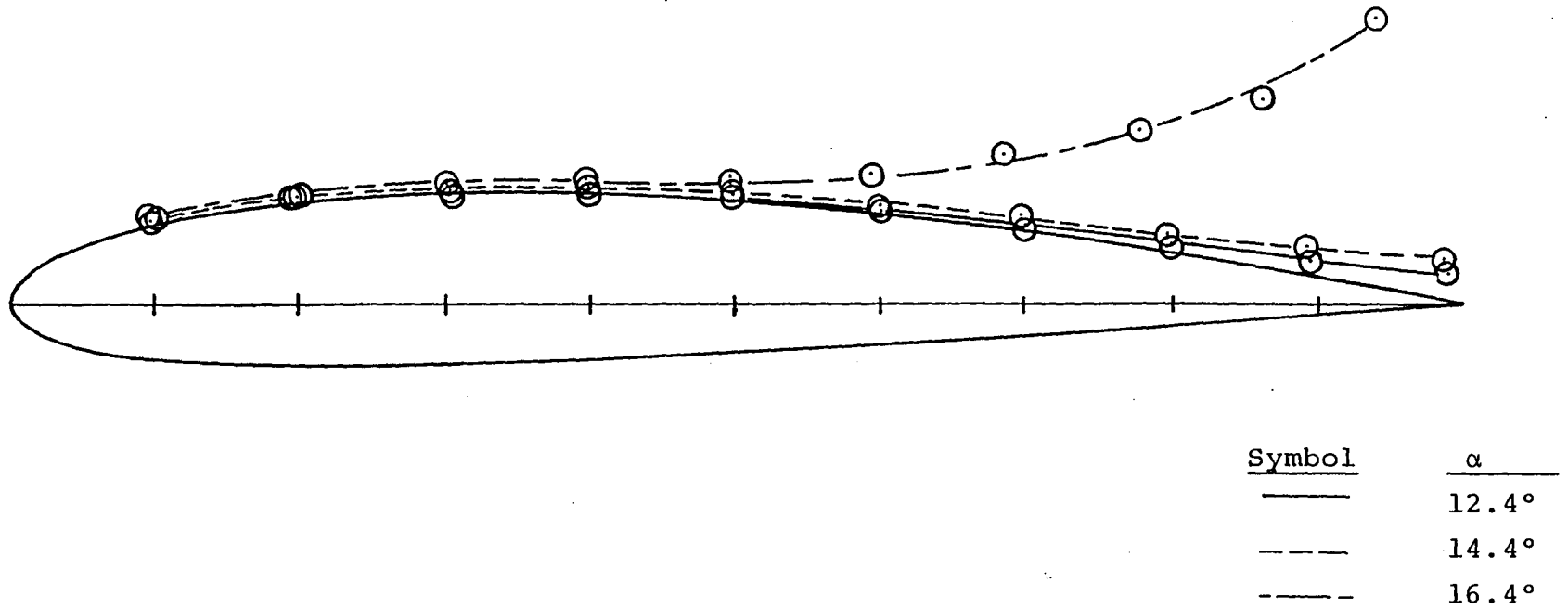


Figure 16 - Boundary Layer Displacement Thickness Distribution.

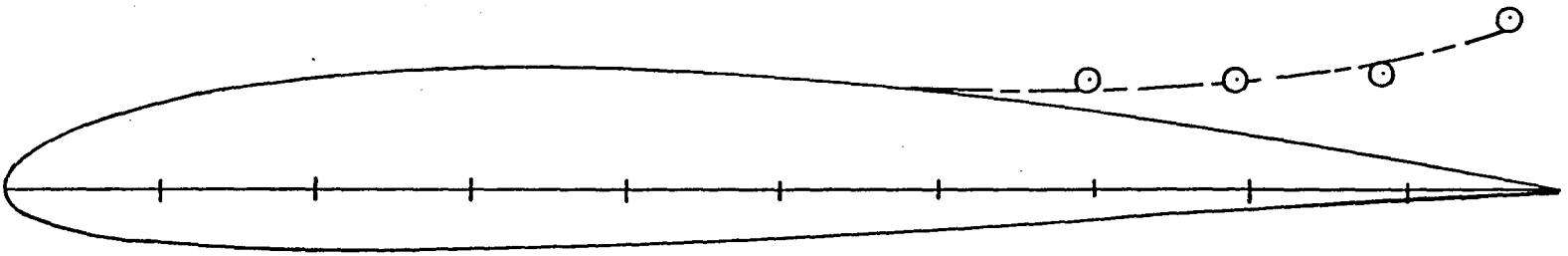
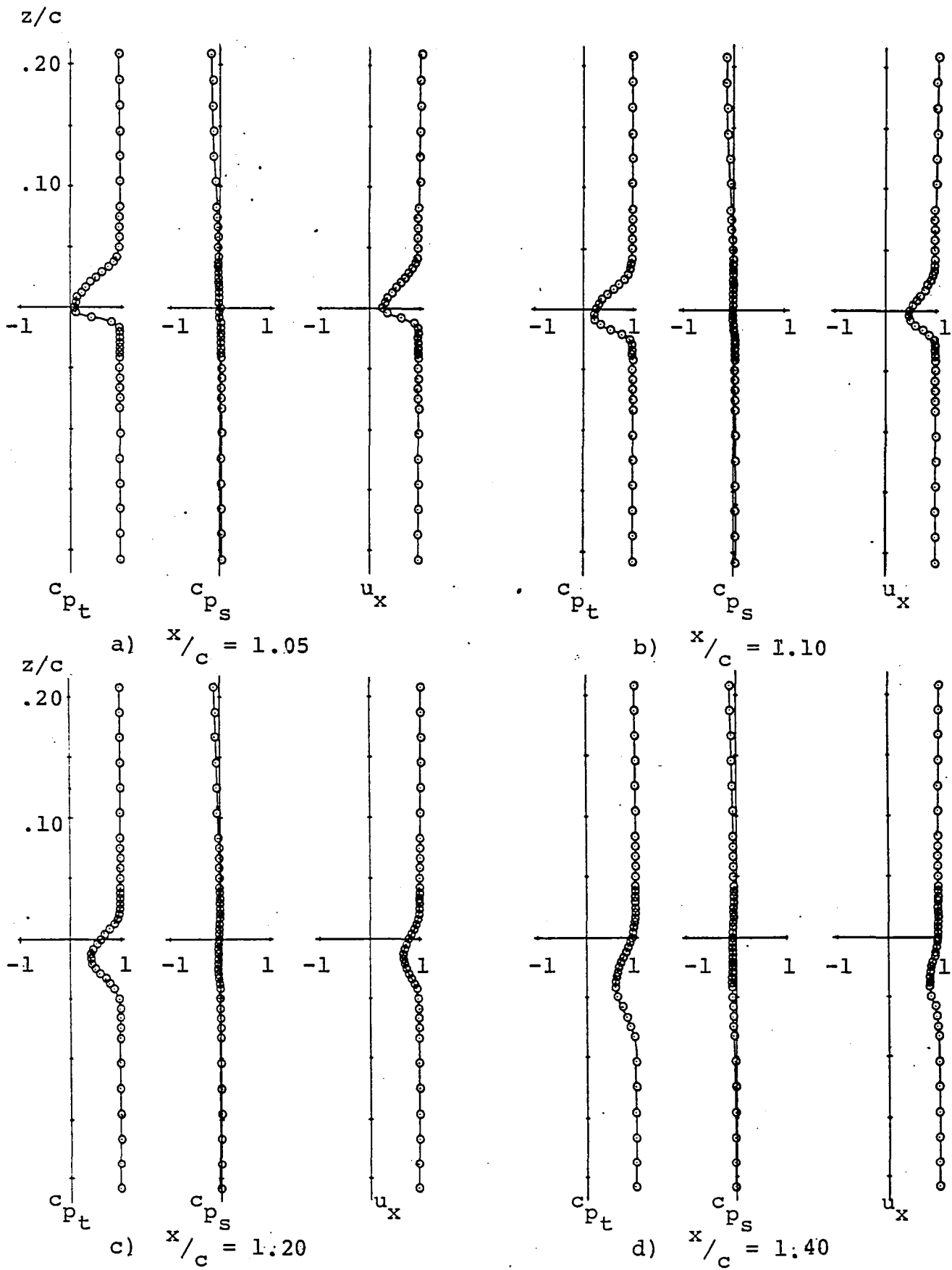
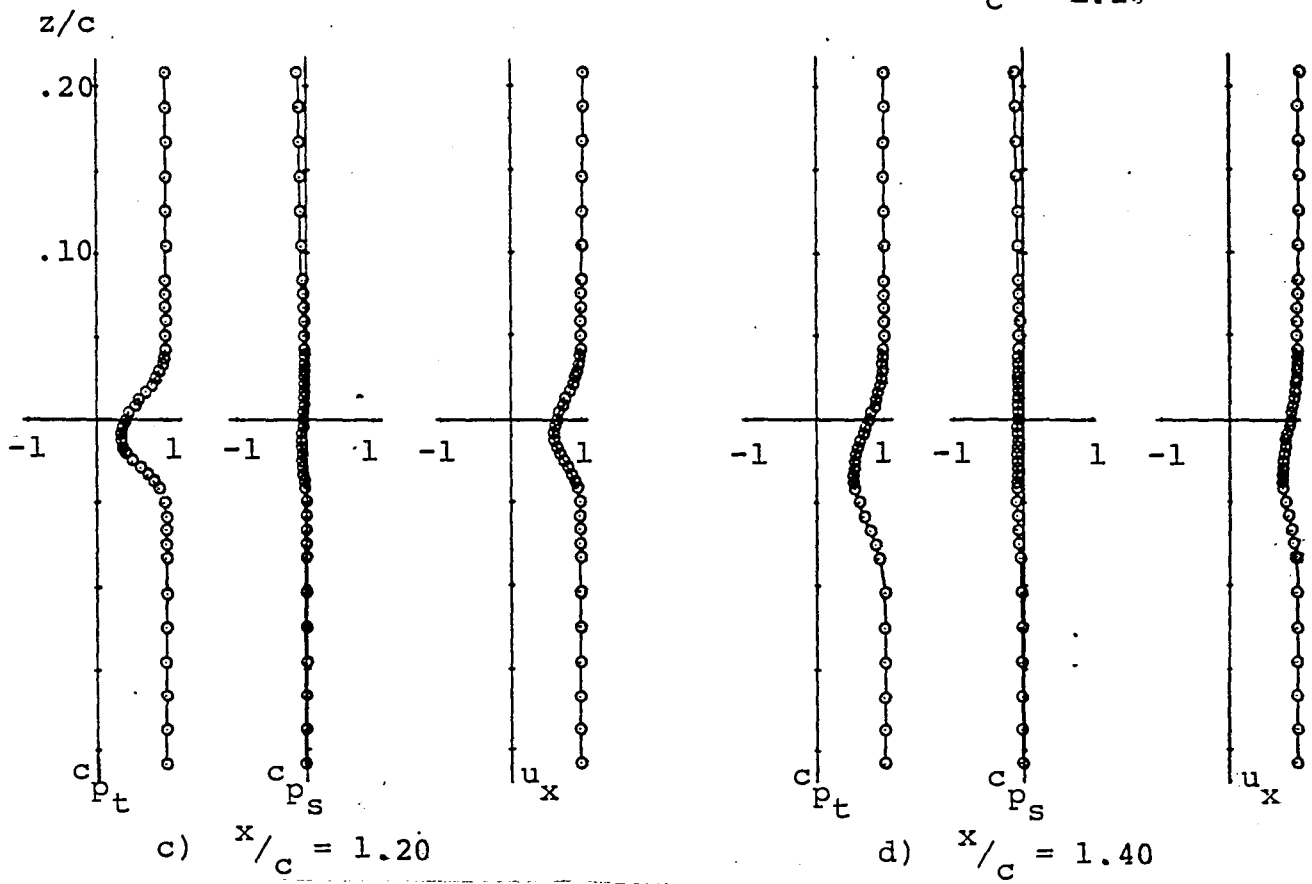
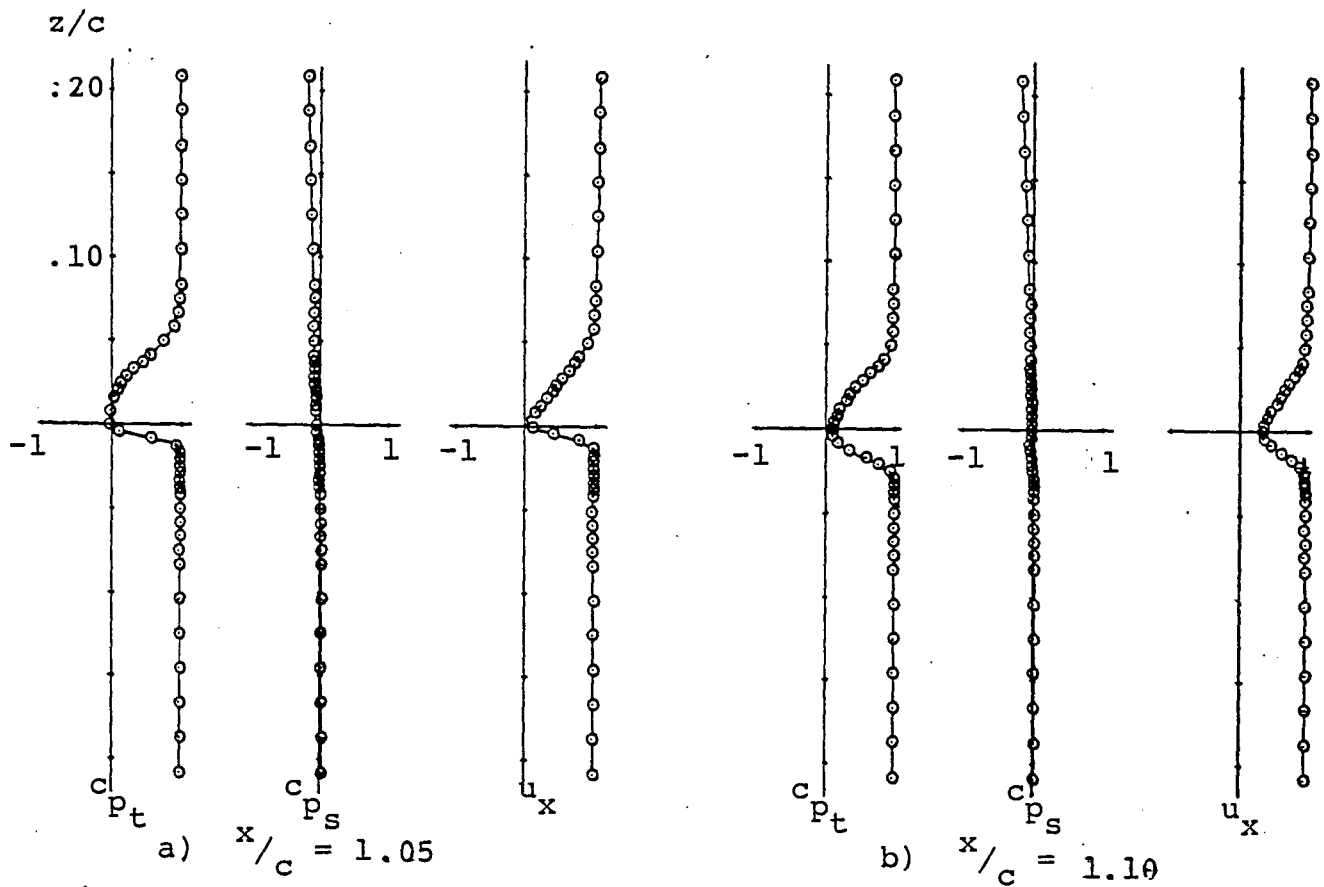


Figure 17 - Separation Streamline,  $\alpha=16.4^\circ$ .



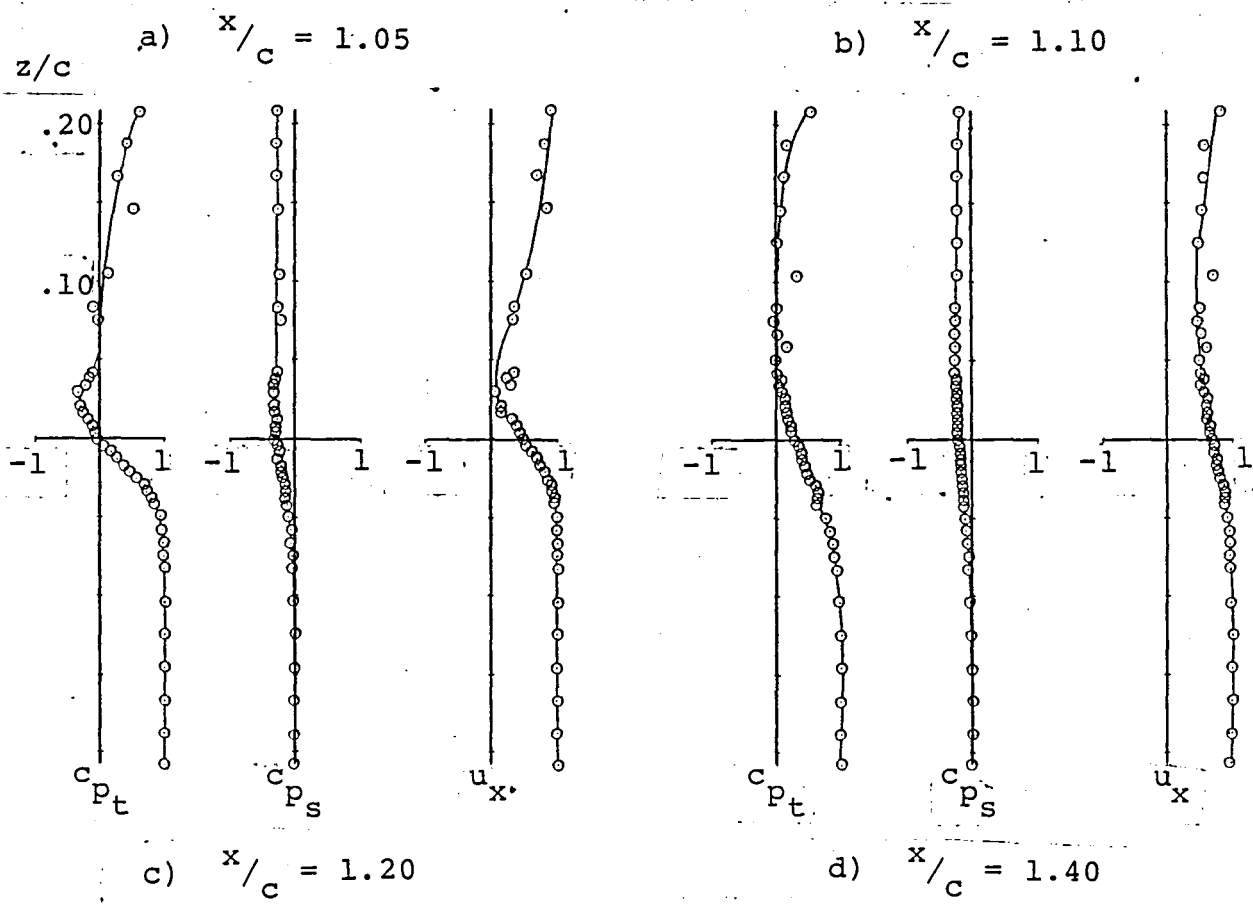
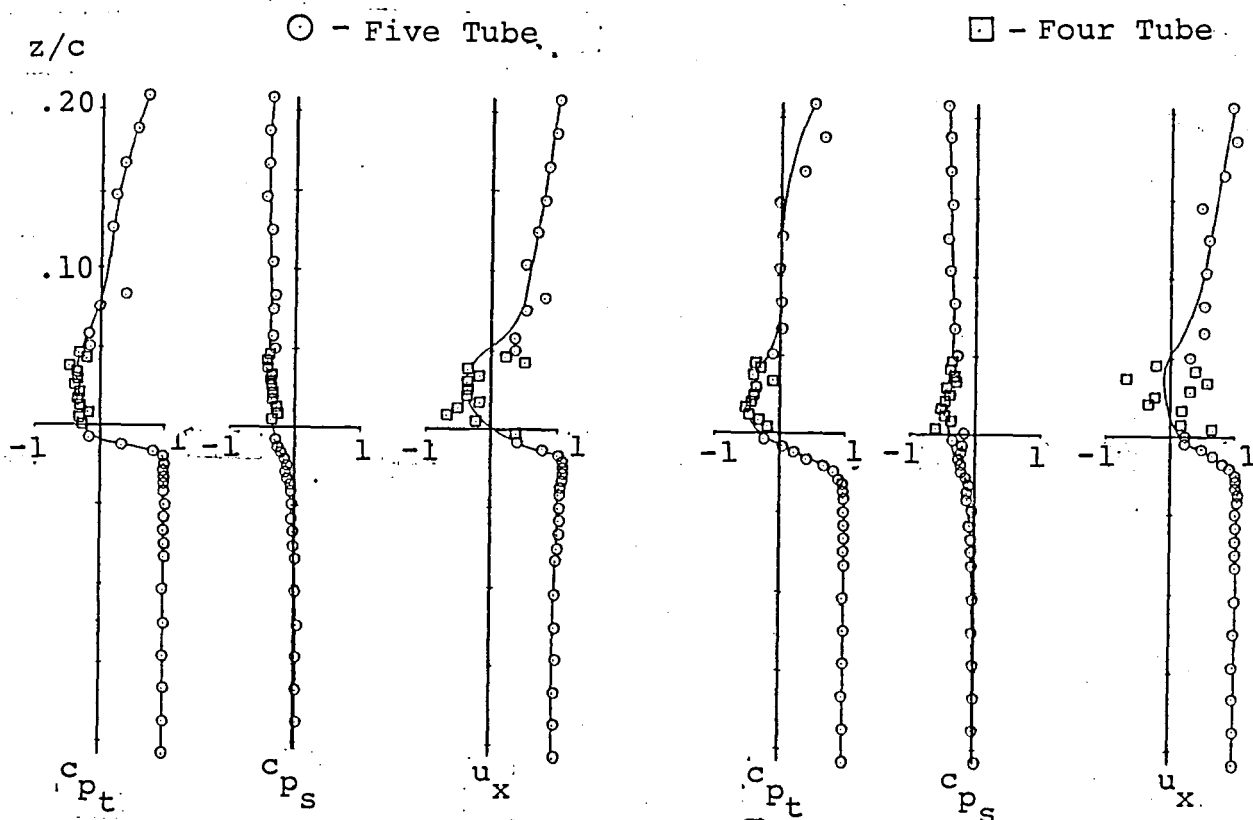
a) Pre-stall angle of attack,  $\alpha = 12.4^\circ$

Figure 18 - Velocity and Pressure Distributions in the Wake.



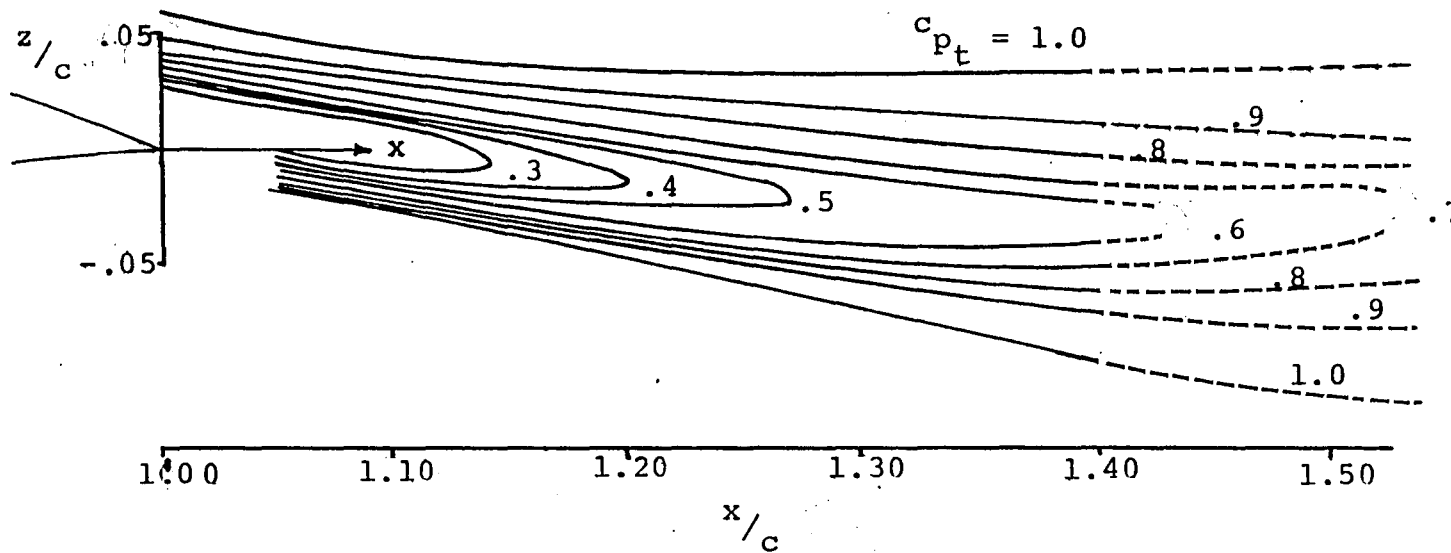
b) Stall angle of attack,  $\alpha = 14.4^\circ$

Figure 18 - Continued.



c) Post-stall angle of attack,  $\alpha = 16.4^\circ$

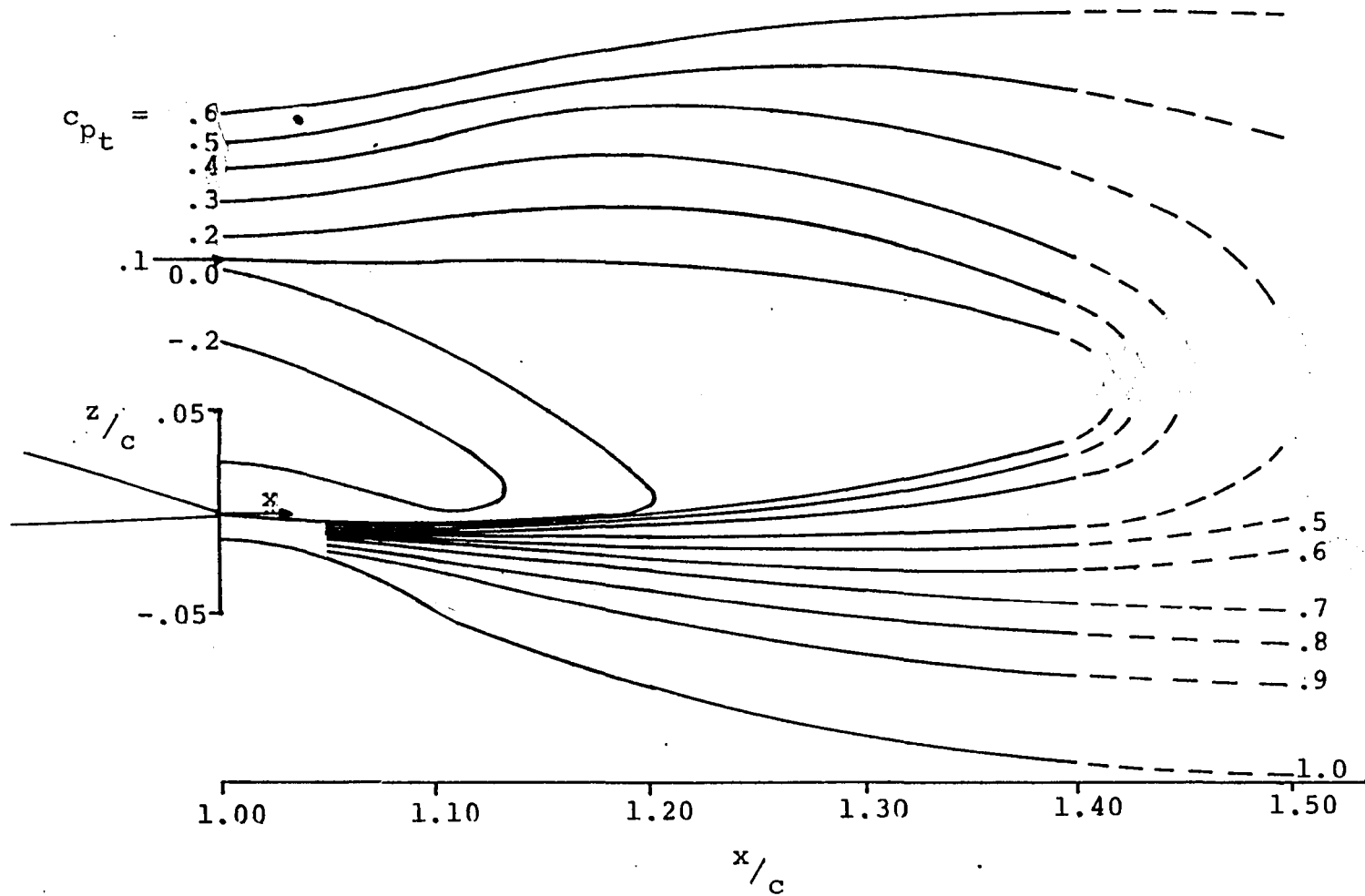
Figure 18 - Concluded.



a) Pre-stall angle of attack,  $\alpha=12.4^\circ$

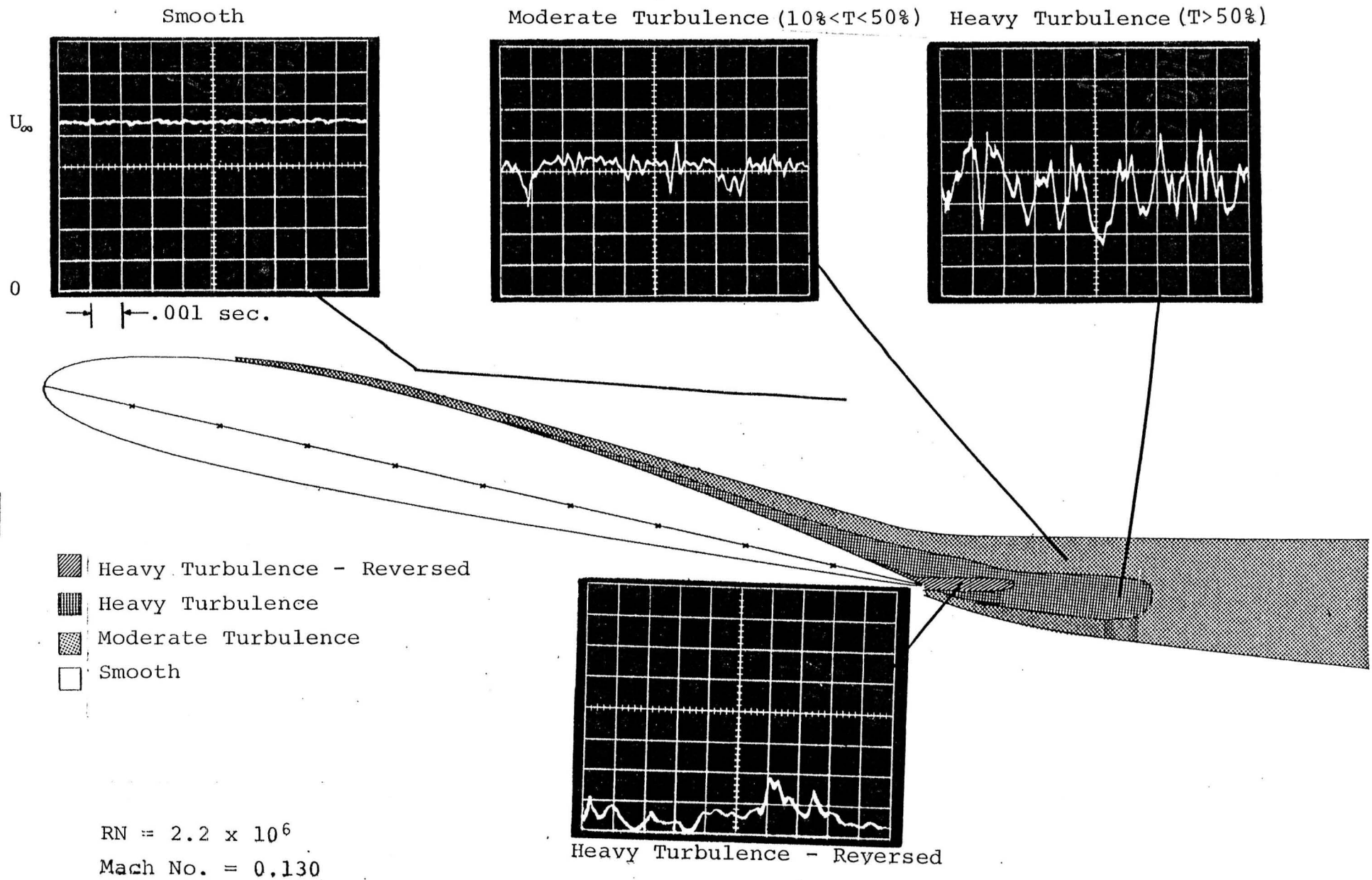
Figure 19 - Wake Total Pressure Contours.





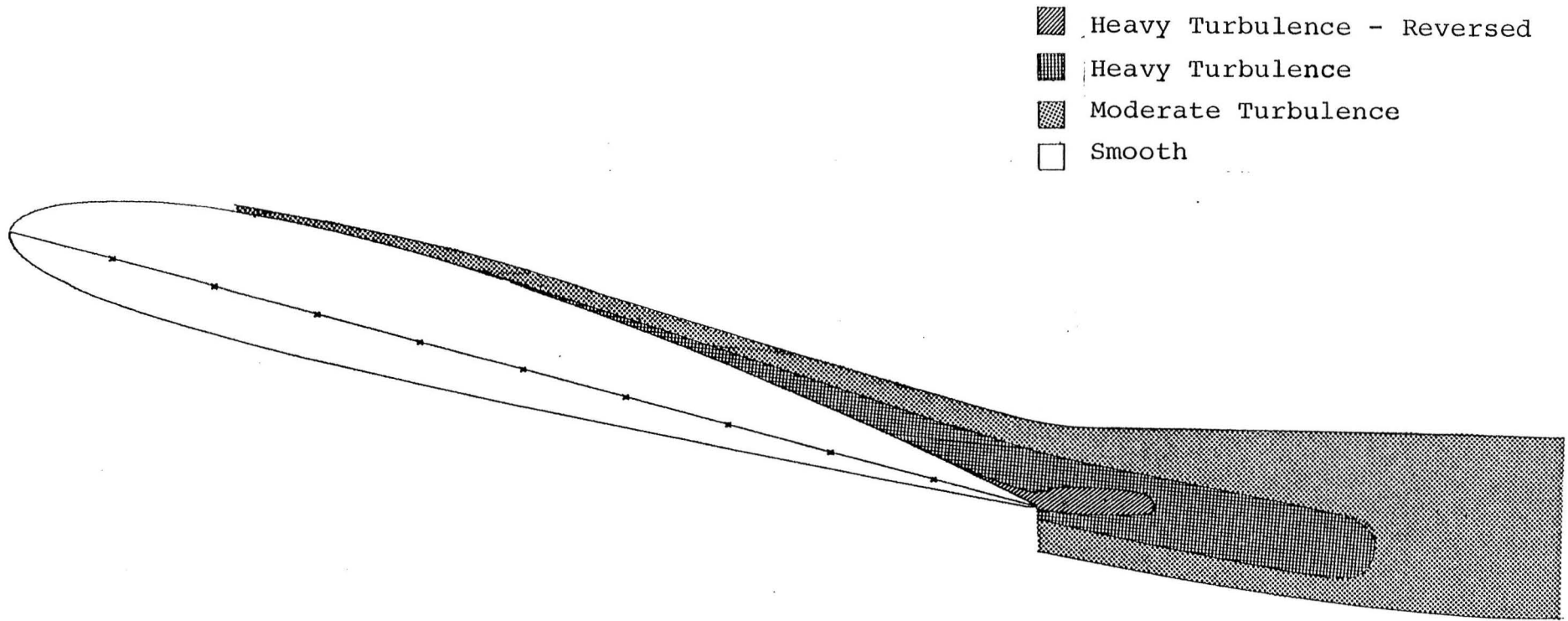
c) Post-stall angle of attack,  $\alpha = 16.4^\circ$

Figure 19 - Concluded.



a) Pre-stall angle of attack,  $\alpha = 12.4^\circ$

Figure 20 - Hot Film Velocity Field Survey.

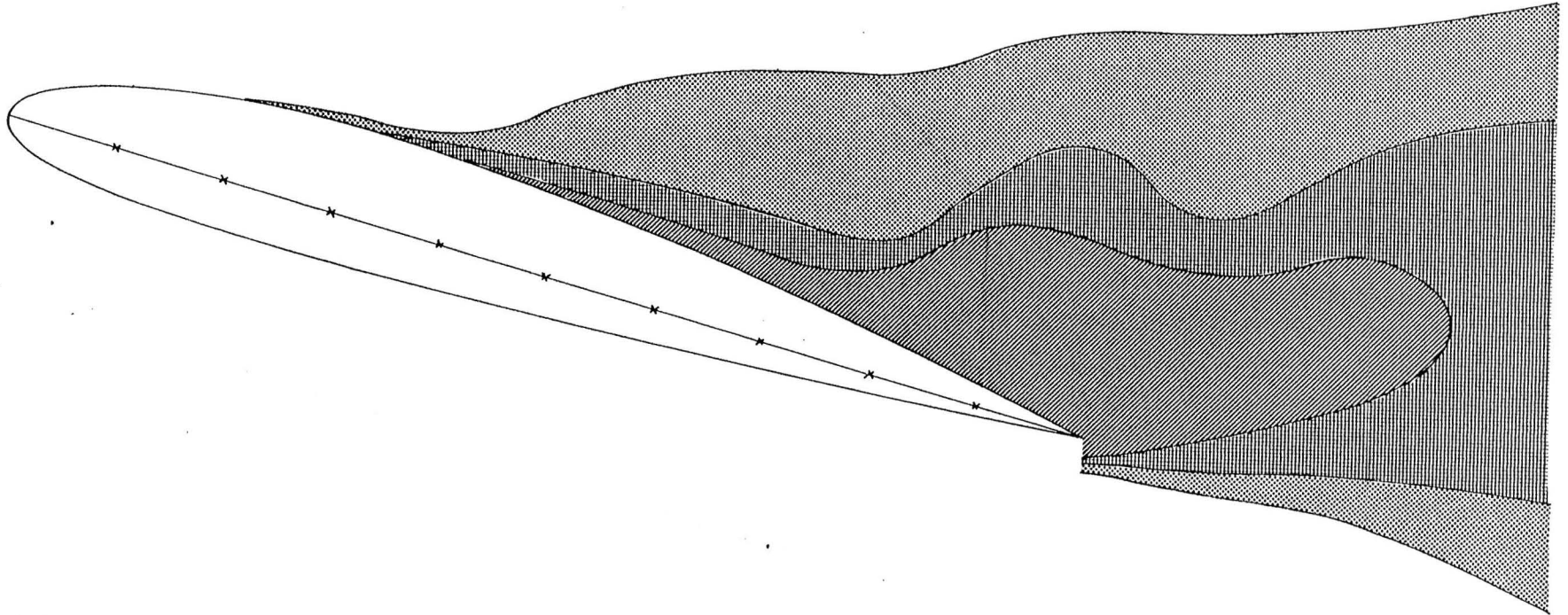


RN =  $2.2 \times 10^6$   
Mach No. = 0.130

b) Stall angle of attack,  $\alpha=14.4^\circ$

Figure 20 - Continued.

- ▨ Heavy Turbulence - Reversed
- ▧ Heavy Turbulence
- ▩ Moderate Turbulence
- Smooth



$Re = 2.2 \times 10^6$   
Mach No. = 0.130

c) Post-stall angle of attack,  $\alpha=16.4^\circ$

Figure 20 - Concluded.

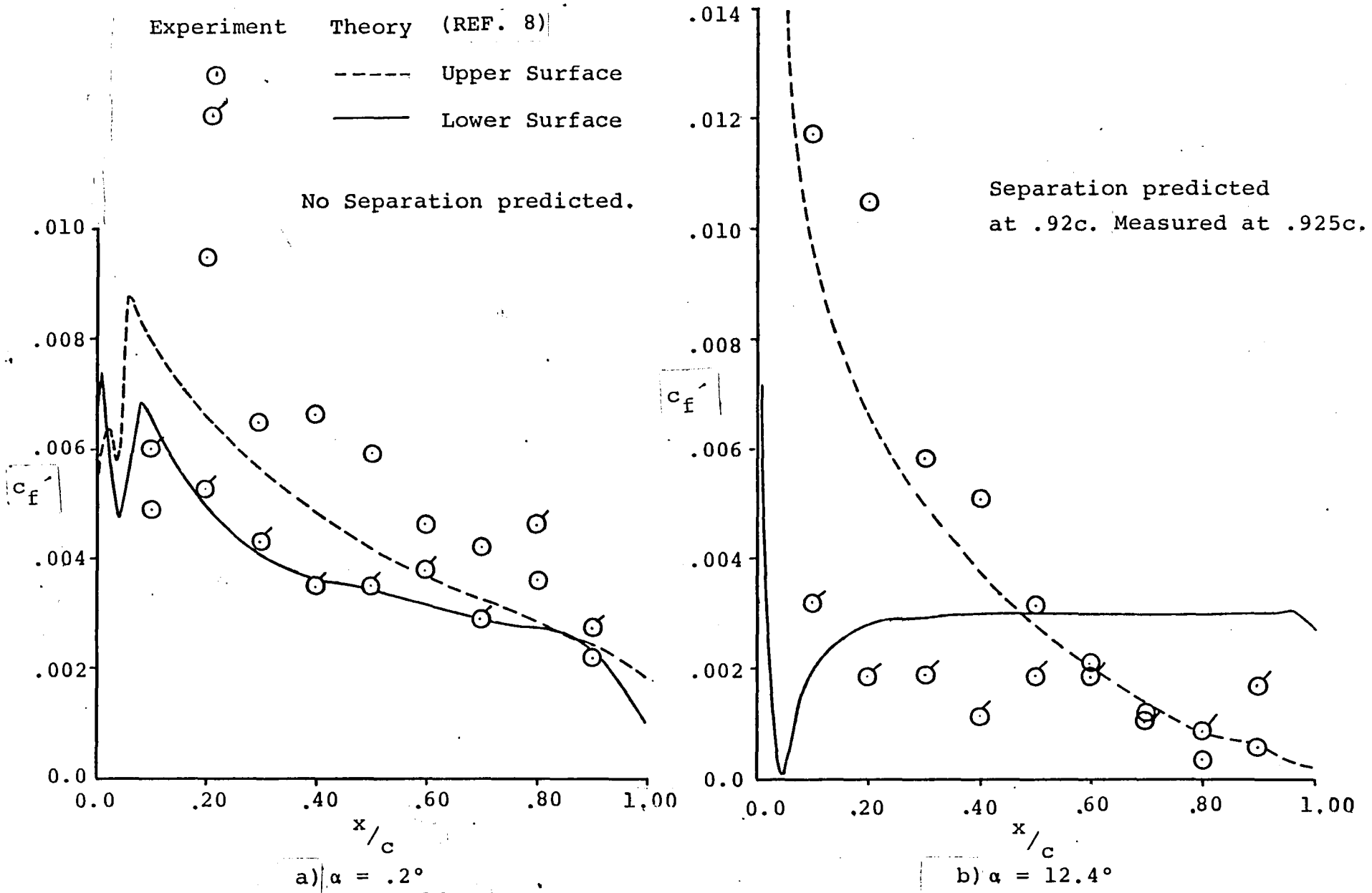


Figure 21 - Comparison of Experimental and Theoretical Skin Friction Distributions.

## APPENDIX A

### Velocity Profiles as Measured by Various Instruments in Unsteady Reversed Flow Fields

In the course of the present investigation, various instrumentation has been developed and used to sense velocity profiles. The flow fields over the airfoil and in the wake are steady for certain angles of attack. For other larger angles of attack, regions of reversed flow accompanied by unsteady flow can occur over the aft portions of the airfoil and in the wake.

Initially a five-tube probe was used for measuring the velocity profiles. However this probe did not accurately sense the regions of reversed flow. Therefore, a four-tube probe was developed and used in the regions where reversed flow existed and regions near the surface of the body. Later the hot film became available and was used primarily to sense the unsteady portions of the flow field and to get the maximum excursions of the velocities. The hot film was also used to sense the regions of flow reversal. As explained in the text, if at any time the flow velocity at some point became zero the flow was deemed to have reversed. Near the end of the present research a split film anemometer was obtained. This allowed sensing of the velocity both in a positive and negative direction and therefore provided a clearer measurement of the reversed flow regions.

As mentioned in the text any pressure probe device such as the four- or five-tube probe cannot respond to rapid fluctuations of the flow field. These probes therefore measure some integrated average depending on the tube size, oscillation frequency, etc. Thus in the regions of unsteady flow some average velocity is measured by the four-tube or the five-tube probe,

whereas, with the split film actual velocity fluctuations are obtained. If a sufficient sample size can be recorded and processed, a true mean velocity can be determined.

Figure A1 shows a comparison of velocity measurements as obtained by the four-tube, five-tube and split film probes at various stations near the aft end of the airfoil. These data were obtained for the 2412 airfoil at an angle of attack of 16.4 degrees. For the split film data, only minimum and maximum values were recorded. These data are shown as the shaded area indicating the maximum and minimum velocities. The dashed line shows the average of the maximum and the minimum and is not the true mean of the time varying velocities. One can see from this figure that the four-tube and five-tube probe measurements show an average velocity somewhere between the maximum and minimum time fluctuating velocities. Thus, one must exercise caution in interpreting the data obtained with the various probes. The present comparison does reflect reasonably good agreement as to the flow reversal points measured by split film and pressure probes.

From this series of tests the advantages of using the split film are evident. High rate digital data acquisition and processing techniques are presently being developed to obtain statistical data associated with the velocity fluctuations such as the maximum and minimum velocities, the mean velocity, turbulence levels, standard deviations, etc. These techniques will be applied as standard testing methods at WSU as they are developed and incorporated in the data reduction computer programs.

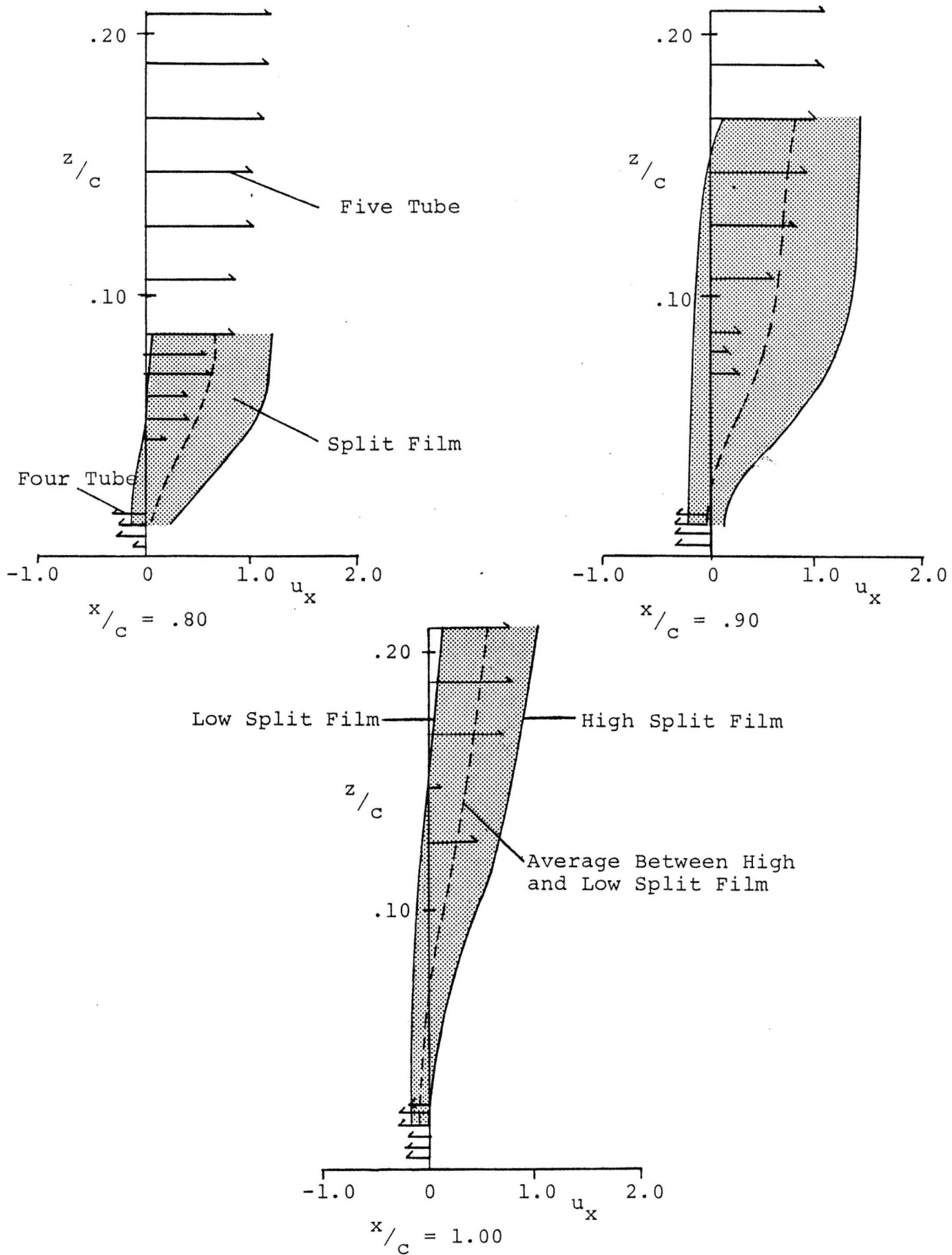


Figure A1 - Velocity Profiles From Various Instruments in Unsteady Reverse Flow.

## Appendix B - Probe Interference Effects on Static Pressure Measurements

During the course of the measurements of the flow properties over airfoils it was found that for certain cases the probe and probe mechanism interfered with the static pressure distribution on the airfoil. This Appendix describes the modifications and calibrations conducted to remedy the problem.

Since interference of this type had not been encountered on tests of the 17% GA(W)-1 airfoil (Ref. B1), special runs were made with the moderate thickness NACA 2412 and GA(W)-2 airfoil sections to identify the source and magnitude of the interference. These runs showed that the interference was significant only at post- $C_{l_{max}}$  angle of attack (see figures B1 through B3).

In order to reduce probe mount interference, a new test section ceiling was designed and installed. The new ceiling had a longitudinal slot and structural provisions for mounting the probe track and carriage above the test section. The ceiling slot opening was fitted with foam seals to prevent leakage, and a new airfoil-shaped probe strut was designed and fabricated to replace the circular strut used in earlier tests. Figure B4 shows a sketch of the probe and probe mechanism in the wind tunnel before and after the modifications.

Figure B5 shows that the static pressure distribution after modification with strut installed is essentially the same as without strut. Tests made with the strut plus probe show that the probe influences the surface pressure distribution somewhat, but does not have a radical influence on apparent separation point location. Thus most of the interference encountered with the original set-up had been eliminated. Based upon these calibrations the installation was judged to be acceptable and detailed flow studies at the post- $C_{l_{max}}$  were conducted with this instrumentation configuration.

Also shown on Figure B5 are the surface static pressure coefficient distributions as obtained from extrapolation of the static pressure profiles of Figure 11. Figures B6 and B7 are plots of the surface static pressure plots as extrapolated for the pre-stall and stall angles of attack and the static pressure as measured by the surface static pressure ports, without probe. These give an indication of the interference errors that exist in the data. For the pre-stall and near-stall angles of attack the discrepancies are quite small. For the post-stall case, the data indicate that the separation point is about  $0.12c$  further downstream with the probe installed. While this shift in separation location is not unacceptably large, it is responsible for fairly large  $C_p$  changes near the separation point. Pressures aft of separation and near the leading edge show negligible changes.

--Reference B1. Seetharam, H.C. and Wentz, W.H., Jr.: Experimental Studies of Flow Separation and Stalling on a Two-Dimensional Airfoil at Low Speeds. NACA CR-2560, July 1975.

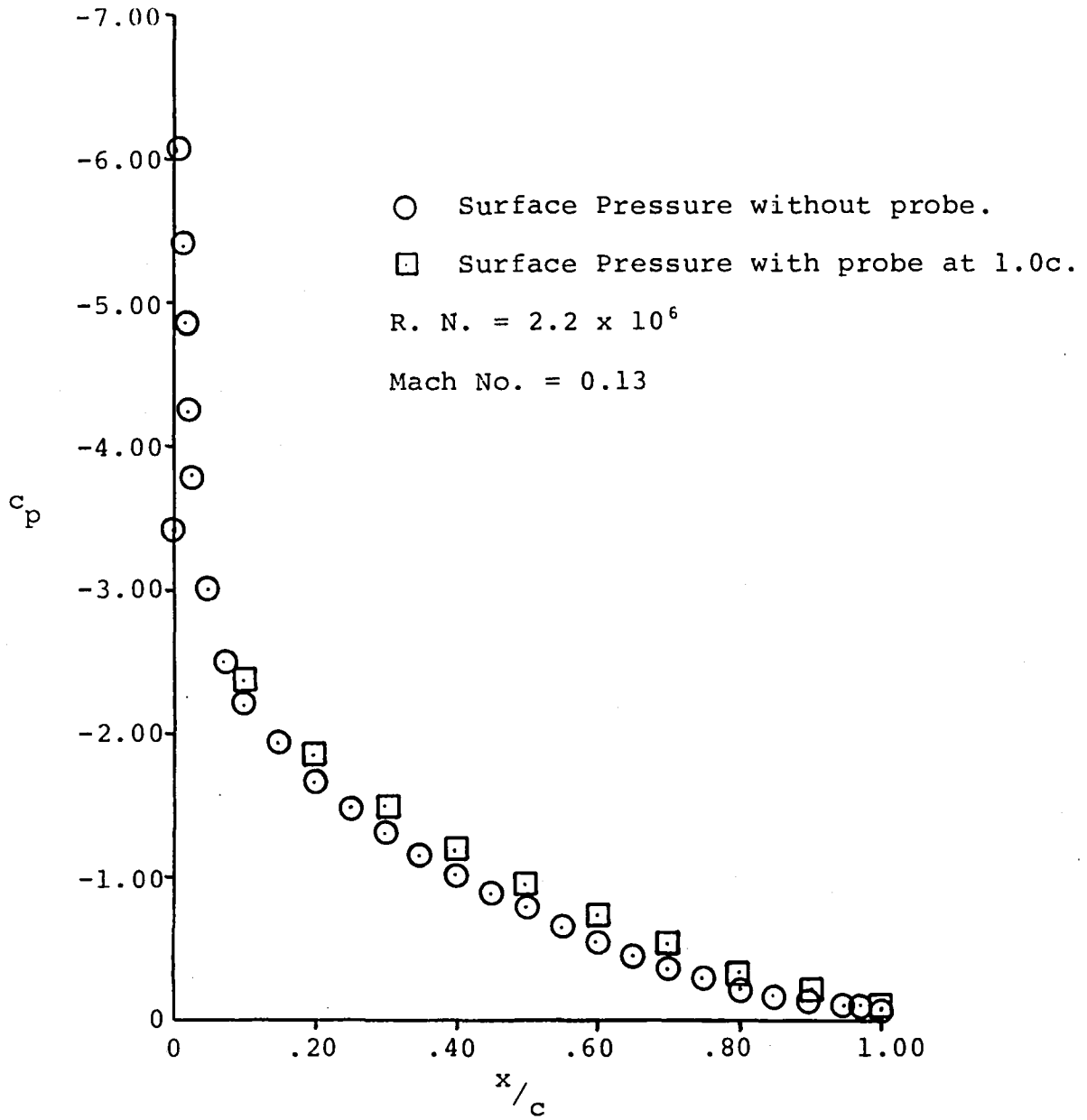


Figure B1 - Calibration for Probe Interference, NACA 2412,  $\alpha=12.4^\circ$ .

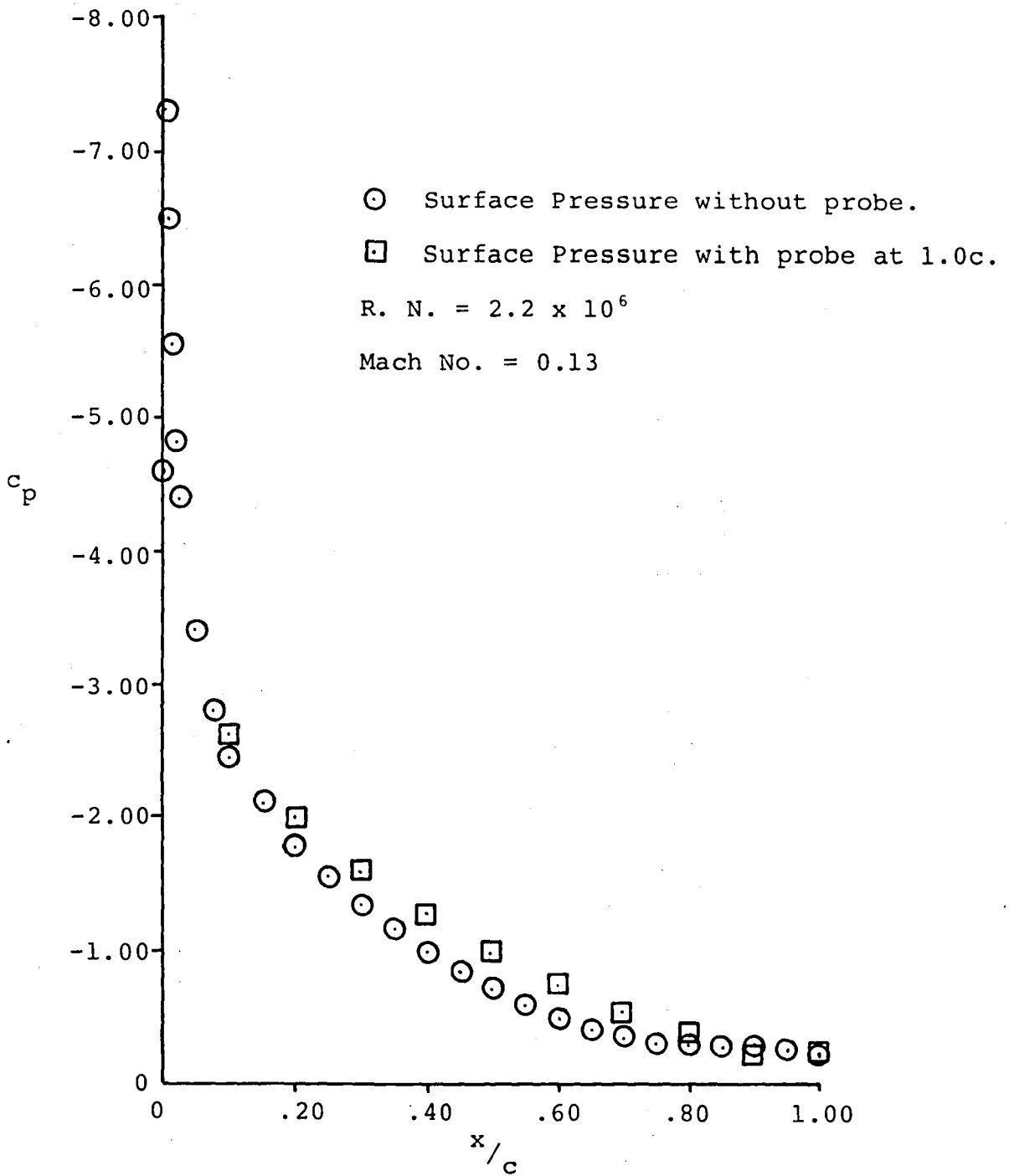


Figure B2 - Calibration for Probe Interference, NACA 2412,  $\alpha=14.4^\circ$ .

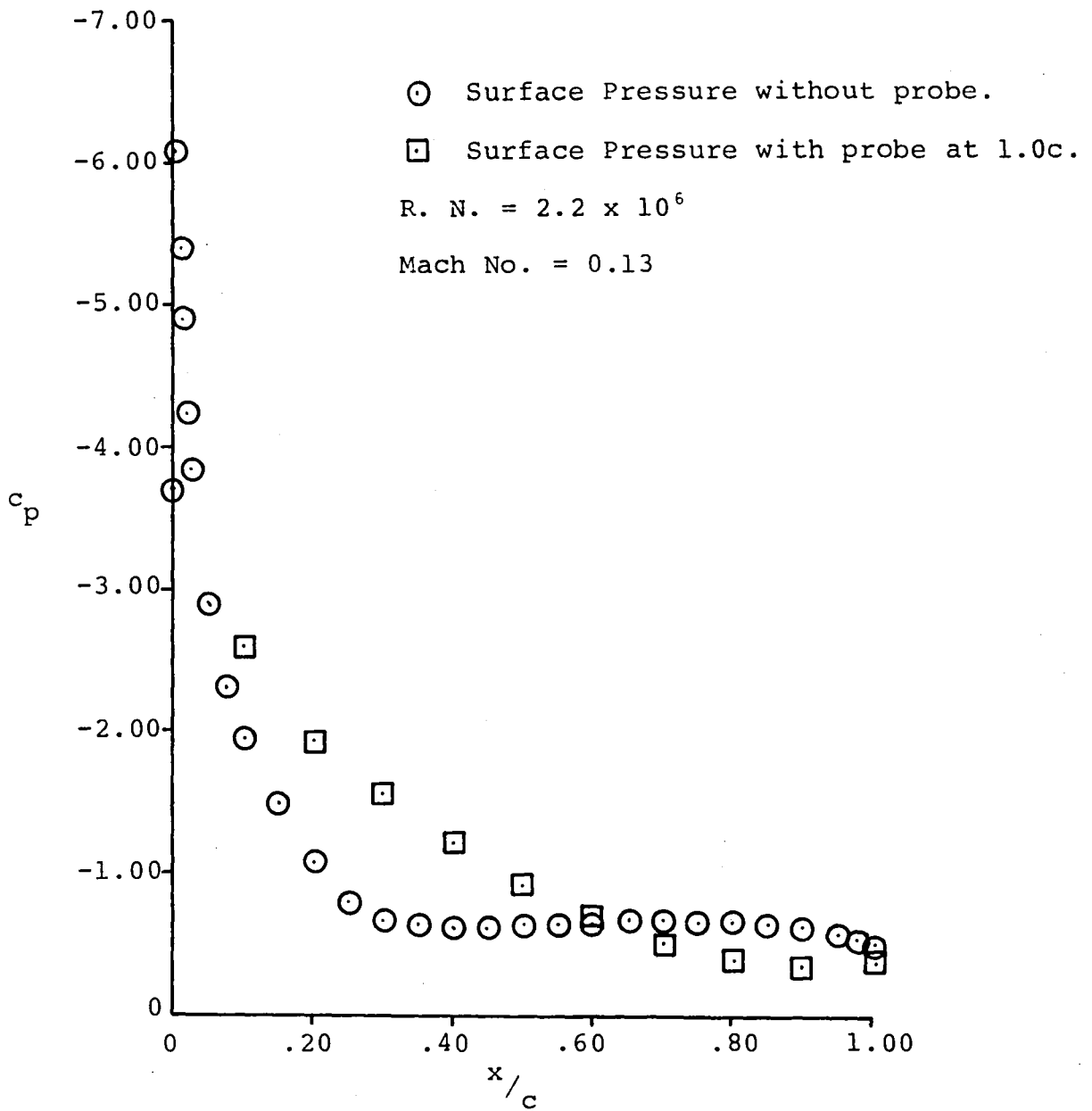
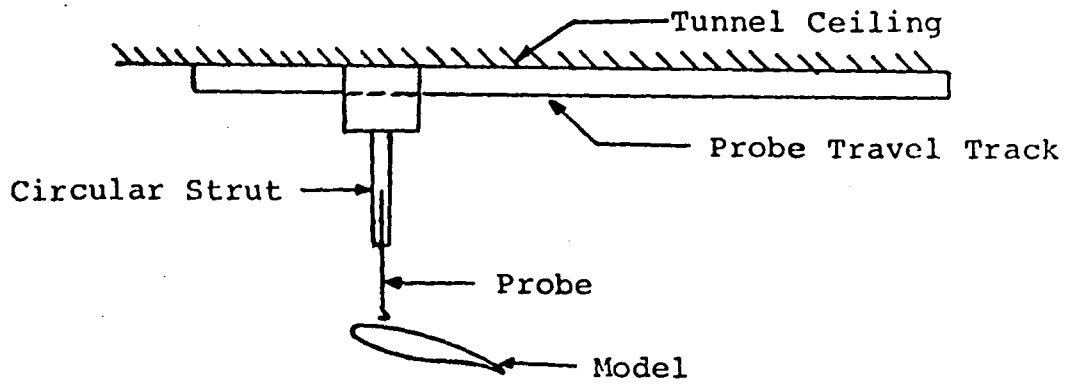
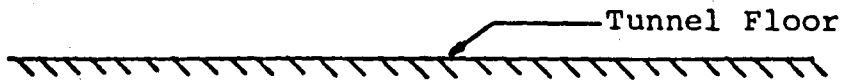
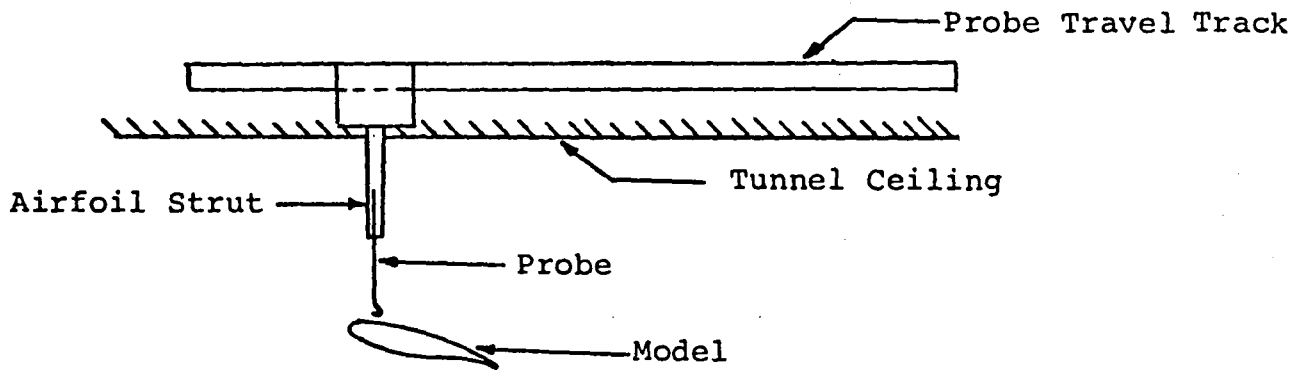


Figure B3 - Calibration for Probe Interference, NACA 2412,  $\alpha=16.4^\circ$ .



a) Before Modification



b) After Modification

Figure B4 - Probe mount and tunnel modifications.

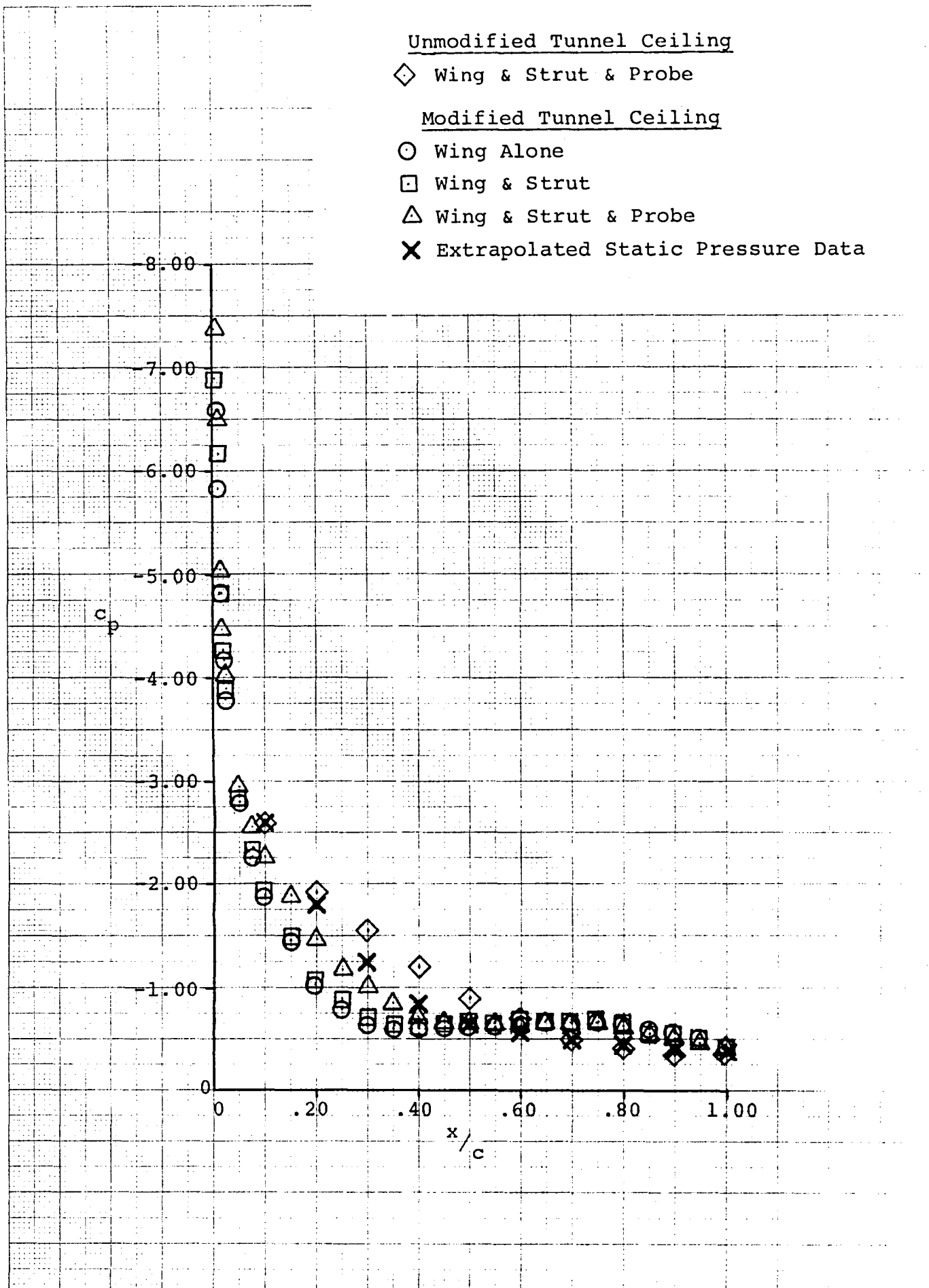


Figure B5 - Surface Static Pressure Interference, NACA 2412,  $\alpha=16.4^\circ$ .

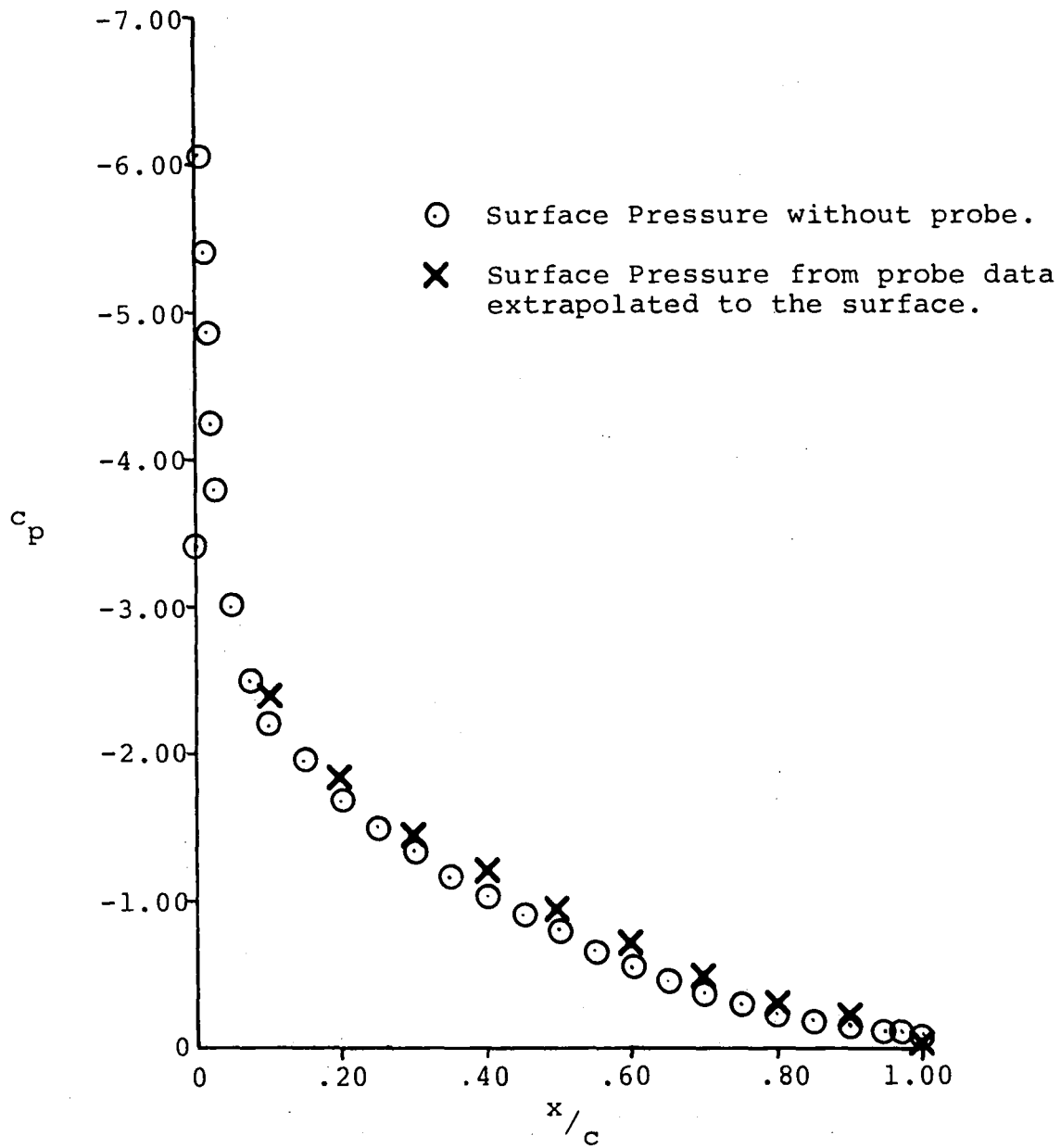


Figure B6 - Surface Static Pressure Interference, NACA 2412,  $\alpha=12.4^\circ$ .

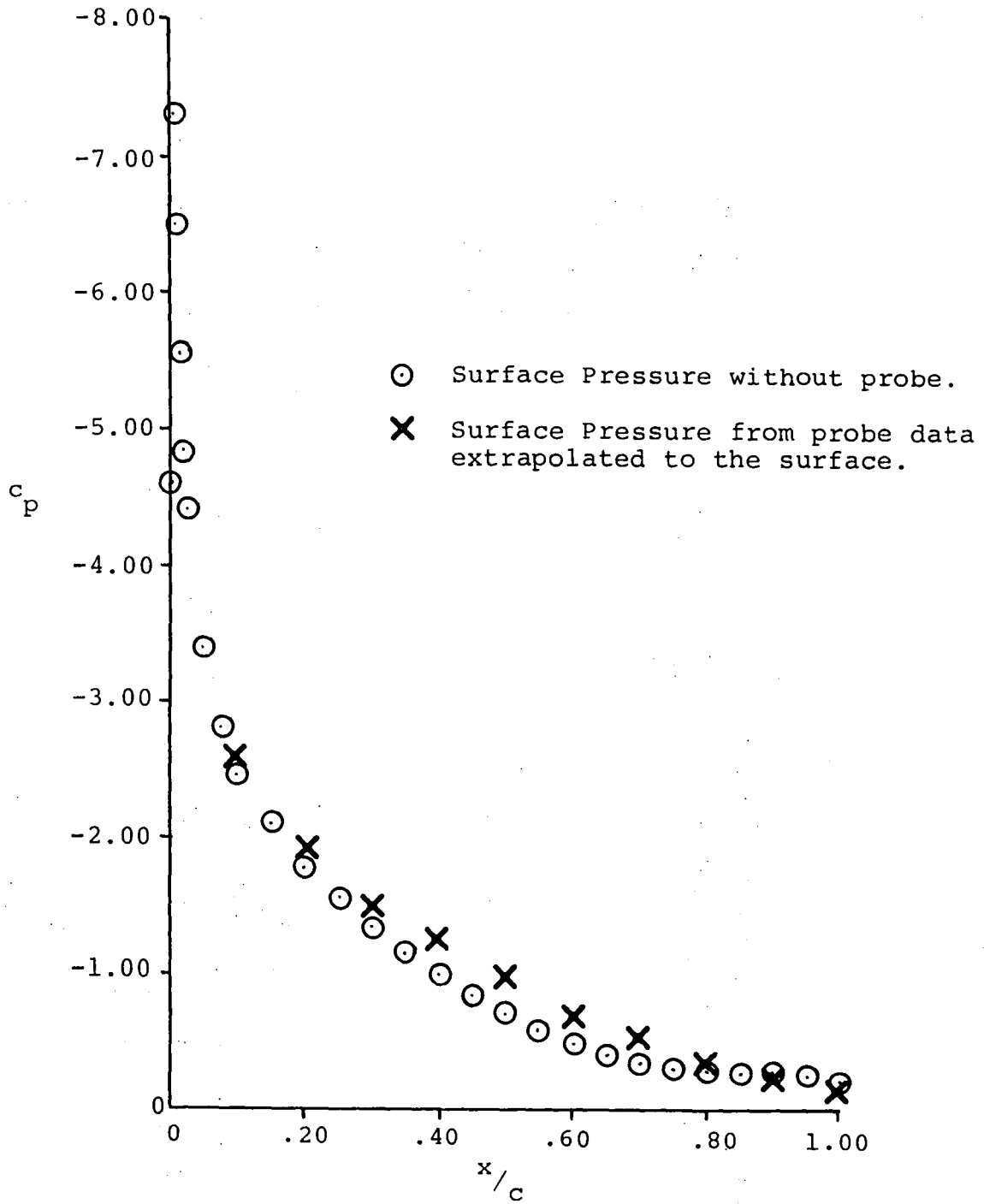


Figure B7 - Surface Static Pressure Interference, NACA 2412,  $\alpha=14.4^\circ$ .

NASA Technical Library



3 1176 01413 7195